

NASA Technical Paper 1138

**Prelaunch Testing of
the Geos-3 Laser Reflector Array**

**CASE FILE
COPY**

**P. O. Minott, M. W. Fitzmaurice,
J. B. Abshire, and H. E. Rowe**

JANUARY 1978

NASA

NASA Technical Paper 1138

Prelaunch Testing of the Geos-3 Laser Reflector Array

P. O. Minott, M. W. Fitzmaurice,
J. B. Abshire, and H. E. Rowe
Goddard Space Flight Center
Greenbelt, Maryland



National Aeronautics
and Space Administration

**Scientific and Technical
Information Office**

1978

This document makes use of international metric units according to the Systeme International d'Unites (SI). In certain cases, utility requires the retention of other systems of units in addition to the SI units. The conventional units stated in parentheses following the computed SI equivalents are the basis of the measurements and calculations reported.

CONTENTS

	<i>Page</i>
INTRODUCTION	1
DESCRIPTION OF THE ARRAY	3
SATELLITE CROSS SECTION	10
TARGET SIGNATURE TESTS	20
ACKNOWLEDGMENTS	34
SOURCES	35
APPENDIX A: CUBE CORNER AND ARRAY SPECIFICATIONS	A-1
APPENDIX B: THE RADAR RANGE EQUATION	B-1
APPENDIX C: IMAGE SCANNER READOUTS	C-1

PRELAUNCH TESTING OF THE GEOS-3 LASER REFLECTOR ARRAY

P. O. Minott, M. W. Fitzmaurice, J. B. Abshire,
and H. E. Rowe
*Goddard Space Flight Center
Greenbelt, Maryland*

INTRODUCTION

This report describes the results of tests performed on the Geodetic Earth Orbiting Satellite (Geos-3) laser retrodirector array to determine its lidar cross section and the distance of the center of gravity of the satellite from the center of gravity of the reflected laser pulses. Tests were performed from January through February 1975 by personnel of the Optics Branch (Code 722) and Laser Data Systems Branch (Code 723) at Goddard Space Flight Center (GSFC). Much of the theory behind these tests is described in the documents listed in the reference section.

The Geos-3 array was designed in early 1971. Previous arrays on Geos-1 and -2 had worked quite successfully but, due to the increasing precision and power of the laser tracking network, an array was desired that would give minimum pulse spreading and could be tracked to within 20 degrees of the horizon. The Geos-1 and -2 arrays were both flat arrays that gave excellent performance at zenith (58×10^6 and 100×10^6 m², respectively). However, these arrays degraded very rapidly with zenith angle and were not useful much beyond 50 degrees, although occasional tracking down to 60 degrees had been recorded. Several design configurations were analyzed with regard to their various trade-offs, and it was decided that the cube corners should be placed in a ring on the surface of a cone with the cone axis coincident with the z or gravity gradient axis of the spacecraft. The trade-off analysis shown in figures 1 and 2 indicated that a 45-degree cone was the best possible compromise and was therefore selected for Geos-3. As shown in the figures, the flat array (0 degrees) gives far superior signal strength near zenith, but quickly degrades. The crossover point at which the 45-degree conical array becomes superior to the flat array occurs at a zenith angle of about 45 degrees. One desirable feature of the 45-degree conical array is that the signal strength is relatively constant over a large range of zenith angles. This occurs because the array has a small cross section where the R⁴ space loss is low, and has a much higher cross section at large zenith angles where the space loss is high. In order to minimize the pulse spreading by the array, it was configured as a thin ring of only three rows of cube corners. The cross section of the point on the ring closest to the laser is, in all cases, much stronger than that of other points on the ring, and this gives rise to a reflected pulse with a sharp rise time and rapid decay that allows accurate ranging. Because of the symmetry and geometry of the array, it produces reflected pulses, the centroid of which can be determined to an accuracy of ± 1 cm. This greatly exceeds the ± 15 -cm accuracy originally desired when the array was designed.

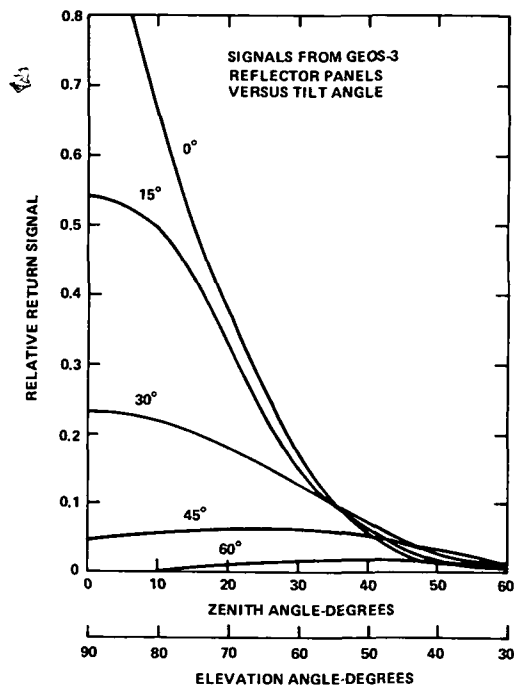


Figure 1. Geos-3 reflector array design, 0° to 60° .

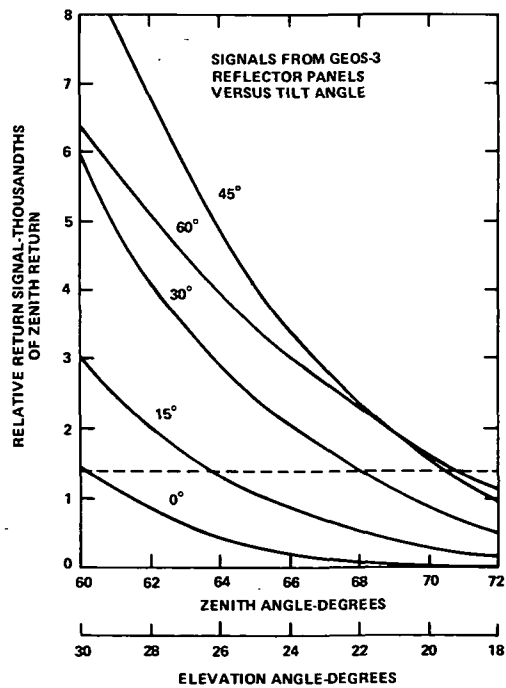


Figure 2. Geos-3 reflector array design, 60° to 72° .

DESCRIPTION OF THE ARRAY

The Geos-3 satellite is shown in figure 3. The satellite is gravity-gradient stabilized and has the following orbital parameters:

Mean Altitude	843 km (500 nmi)
Inclination	115 degrees
Eccentricity	0.006 (maximum)
Orbit Period	101.8 minutes

The cube corners are mounted in a 45-degree conical ring located around the periphery of the Earth-facing side of the spacecraft. The array consists of 264 cube corners whose positions are listed with respect to the satellite center of mass in table 1. The position refers to the position of the vertex of the cube corner. The cube corners are fused silica with a 3.5-cm hexagonal entrance pupil. Reflective faces are silvered, and the dihedrals are 90 degrees. The array configuration is included in Appendix A.



Figure 3. Geos-3 satellite.

Table 1

Cube Corner Position Copy from RETRO Report

CUBE CORNER	CARTESIAN COORDINATES			SPHERICAL COORDINATES			DISTANCES-METERS			ANGLES-DEGREES			ORIENTATION ANGLES			
	X	Y	Z	R	THETA	PHI	C	PHI	THETA	N	PHI	GAMMA	THETA	N	PHI	GAMMA
1	0.5225	0.0187	1.3371	1.4357	21.358	2.045	45.000	2.045	45.000	2.045	0.0	2.045	45.000	2.045	0.0	0.0
2	0.5139	0.0559	1.3371	1.4357	21.358	6.136	45.000	6.136	45.000	6.136	0.0	6.136	45.000	6.136	0.0	0.0
3	0.5146	0.0928	1.3371	1.4357	21.358	10.227	45.000	10.227	45.000	10.227	0.0	10.227	45.000	10.227	0.0	0.0
4	0.5066	0.1293	1.3371	1.4357	21.358	14.318	45.000	14.318	45.000	14.318	0.0	14.318	45.000	14.318	0.0	0.0
5	0.4961	0.1651	1.3371	1.4357	21.358	18.409	45.000	18.409	45.000	18.409	0.0	18.409	45.000	18.409	0.0	0.0
6	0.4831	0.2001	1.3371	1.4357	21.358	22.500	45.000	22.500	45.000	22.500	0.0	22.500	45.000	22.500	0.0	0.0
7	0.4676	0.2340	1.3371	1.4357	21.358	26.591	45.000	26.591	45.000	26.591	0.0	26.591	45.000	26.591	0.0	0.0
8	0.4497	0.2668	1.3371	1.4357	21.358	30.682	45.000	30.682	45.000	30.682	0.0	30.682	45.000	30.682	0.0	0.0
9	0.4295	0.2982	1.3371	1.4357	21.358	34.773	45.000	34.773	45.000	34.773	0.0	34.773	45.000	34.773	0.0	0.0
10	0.4071	0.3291	1.3371	1.4357	21.358	38.864	45.000	38.864	45.000	38.864	0.0	38.864	45.000	38.864	0.0	0.0
11	0.3827	0.3583	1.3371	1.4357	21.358	42.955	45.000	42.955	45.000	42.955	0.0	42.955	45.000	42.955	0.0	0.0
12	0.3563	0.3827	1.3371	1.4357	21.358	47.045	45.000	47.045	45.000	47.045	0.0	47.045	45.000	47.045	0.0	0.0
13	0.3281	0.4021	1.3371	1.4357	21.358	51.136	45.000	51.136	45.000	51.136	0.0	51.136	45.000	51.136	0.0	0.0
14	0.2982	0.4295	1.3371	1.4357	21.358	55.227	45.000	55.227	45.000	55.227	0.0	55.227	45.000	55.227	0.0	0.0
15	0.2668	0.4497	1.3371	1.4357	21.358	59.318	45.000	59.318	45.000	59.318	0.0	59.318	45.000	59.318	0.0	0.0
16	0.2340	0.4676	1.3371	1.4357	21.358	63.409	45.000	63.409	45.000	63.409	0.0	63.409	45.000	63.409	0.0	0.0
17	0.2001	0.4831	1.3371	1.4357	21.358	67.500	45.000	67.500	45.000	67.500	0.0	67.500	45.000	67.500	0.0	0.0
18	0.1651	0.4961	1.3371	1.4357	21.358	71.591	45.000	71.591	45.000	71.591	0.0	71.591	45.000	71.591	0.0	0.0
19	0.1293	0.5066	1.3371	1.4357	21.358	75.682	45.000	75.682	45.000	75.682	0.0	75.682	45.000	75.682	0.0	0.0
20	0.0928	0.5146	1.3371	1.4357	21.358	79.773	45.000	79.773	45.000	79.773	0.0	79.773	45.000	79.773	0.0	0.0
21	0.0559	0.5199	1.3371	1.4357	21.358	83.864	45.000	83.864	45.000	83.864	0.0	83.864	45.000	83.864	0.0	0.0
22	0.0187	0.5225	1.3371	1.4357	21.358	87.955	45.000	87.955	45.000	87.955	0.0	87.955	45.000	87.955	0.0	0.0
23	-0.0187	0.5199	1.3371	1.4357	21.358	92.045	45.000	92.045	45.000	92.045	0.0	92.045	45.000	92.045	0.0	0.0
24	-0.0559	0.5146	1.3371	1.4357	21.358	96.136	45.000	96.136	45.000	96.136	0.0	96.136	45.000	96.136	0.0	0.0
25	-0.0928	0.5066	1.3371	1.4357	21.358	100.227	45.000	100.227	45.000	100.227	0.0	100.227	45.000	100.227	0.0	0.0
26	-0.1293	0.4961	1.3371	1.4357	21.358	104.318	45.000	104.318	45.000	104.318	0.0	104.318	45.000	104.318	0.0	0.0
27	-0.1651	0.4831	1.3371	1.4357	21.358	108.409	45.000	108.409	45.000	108.409	0.0	108.409	45.000	108.409	0.0	0.0
28	-0.2001	0.4676	1.3371	1.4357	21.358	112.500	45.000	112.500	45.000	112.500	0.0	112.500	45.000	112.500	0.0	0.0
29	-0.2340	0.4497	1.3371	1.4357	21.358	116.591	45.000	116.591	45.000	116.591	0.0	116.591	45.000	116.591	0.0	0.0
30	-0.2668	0.4295	1.3371	1.4357	21.358	120.682	45.000	120.682	45.000	120.682	0.0	120.682	45.000	120.682	0.0	0.0
31	-0.2982	0.4071	1.3371	1.4357	21.358	124.773	45.000	124.773	45.000	124.773	0.0	124.773	45.000	124.773	0.0	0.0
32	-0.3281	0.3827	1.3371	1.4357	21.358	128.864	45.000	128.864	45.000	128.864	0.0	128.864	45.000	128.864	0.0	0.0
33	-0.3563	0.3583	1.3371	1.4357	21.358	132.955	45.000	132.955	45.000	132.955	0.0	132.955	45.000	132.955	0.0	0.0
34	-0.3827	0.3327	1.3371	1.4357	21.358	137.045	45.000	137.045	45.000	137.045	0.0	137.045	45.000	137.045	0.0	0.0
35	-0.4071	0.3063	1.3371	1.4357	21.358	141.136	45.000	141.136	45.000	141.136	0.0	141.136	45.000	141.136	0.0	0.0
36	-0.4295	0.2793	1.3371	1.4357	21.358	145.227	45.000	145.227	45.000	145.227	0.0	145.227	45.000	145.227	0.0	0.0
37	-0.4497	0.2568	1.3371	1.4357	21.358	149.318	45.000	149.318	45.000	149.318	0.0	149.318	45.000	149.318	0.0	0.0
38	-0.4676	0.2340	1.3371	1.4357	21.358	153.409	45.000	153.409	45.000	153.409	0.0	153.409	45.000	153.409	0.0	0.0
39	-0.4831	0.2001	1.3371	1.4357	21.358	157.500	45.000	157.500	45.000	157.500	0.0	157.500	45.000	157.500	0.0	0.0
40	-0.4961	0.1651	1.3371	1.4357	21.358	161.591	45.000	161.591	45.000	161.591	0.0	161.591	45.000	161.591	0.0	0.0
41	-0.5066	0.1293	1.3371	1.4357	21.358	165.682	45.000	165.682	45.000	165.682	0.0	165.682	45.000	165.682	0.0	0.0
42	-0.5146	0.0928	1.3371	1.4357	21.358	169.773	45.000	169.773	45.000	169.773	0.0	169.773	45.000	169.773	0.0	0.0
43	-0.5199	0.0559	1.3371	1.4357	21.358	173.864	45.000	173.864	45.000	173.864	0.0	173.864	45.000	173.864	0.0	0.0
44	-0.5225	0.0187	1.3371	1.4357	21.358	177.955	45.000	177.955	45.000	177.955	0.0	177.955	45.000	177.955	0.0	0.0
45	-0.5281	-0.0187	1.3371	1.4357	21.358	182.045	45.000	182.045	45.000	182.045	0.0	182.045	45.000	182.045	0.0	0.0
46	-0.5199	-0.0559	1.3371	1.4357	21.358	186.136	45.000	186.136	45.000	186.136	0.0	186.136	45.000	186.136	0.0	0.0
47	-0.5146	-0.0928	1.3371	1.4357	21.358	190.227	45.000	190.227	45.000	190.227	0.0	190.227	45.000	190.227	0.0	0.0
48	-0.5066	-0.1293	1.3371	1.4357	21.358	194.318	45.000	194.318	45.000	194.318	0.0	194.318	45.000	194.318	0.0	0.0
49	-0.4961	-0.1651	1.3371	1.4357	21.358	198.409	45.000	198.409	45.000	198.409	0.0	198.409	45.000	198.409	0.0	0.0
50	-0.4831	-0.2001	1.3371	1.4357	21.358	202.500	45.000	202.500	45.000	202.500	0.0	202.500	45.000	202.500	0.0	0.0

Table 1 (Continued)

CUBE CORNER	CARTESIAN COORDINATES			SPHERICAL COORDINATES			DISTANCES-METERS			ANGLES-DEGREES		
	X	Y	Z	R	THETA C	PHI C	THETA N	PHI N	GAMMA	ORIENTATION ANGLES		
										PHI	GAMMA	
51	-0.4676	-0.2340	1.3371	1.4357	21.358	206.591	45.000	206.591	0.0	0.0		
52	-0.4357	-0.2668	1.3371	1.4357	21.358	210.582	45.000	210.582	0.0	0.0		
53	-0.4295	-0.2982	1.3371	1.4357	21.358	214.773	45.000	214.773	0.0	0.0		
54	-0.4071	-0.3281	1.3371	1.4357	21.358	218.864	45.000	218.864	0.0	0.0		
55	-0.3827	-0.3563	1.3371	1.4357	21.358	222.955	45.000	222.955	0.0	0.0		
56	-0.3563	-0.3827	1.3371	1.4357	21.358	227.045	45.000	227.045	0.0	0.0		
57	-0.3281	-0.4071	1.3371	1.4357	21.358	231.136	45.000	231.136	0.0	0.0		
58	-0.2982	-0.4295	1.3371	1.4357	21.358	235.227	45.000	235.227	0.0	0.0		
59	-0.2668	-0.4497	1.3371	1.4357	21.358	239.318	45.000	239.318	0.0	0.0		
60	-0.2340	-0.4676	1.3371	1.4357	21.358	243.409	45.000	243.409	0.0	0.0		
61	-0.2001	-0.4831	1.3371	1.4357	21.358	247.500	45.000	247.500	0.0	0.0		
62	-0.1651	-0.4961	1.3371	1.4357	21.358	251.591	45.000	251.591	0.0	0.0		
63	-0.1293	-0.5066	1.3371	1.4357	21.358	255.682	45.000	255.682	0.0	0.0		
64	-0.0928	-0.5146	1.3371	1.4357	21.358	259.773	45.000	259.773	0.0	0.0		
65	-0.0559	-0.5199	1.3371	1.4357	21.358	263.864	45.000	263.864	0.0	0.0		
66	-0.0187	-0.5222	1.3371	1.4357	21.358	267.954	45.000	267.954	0.0	0.0		
67	0.0187	-0.5225	1.3371	1.4357	21.358	272.045	45.000	272.045	0.0	0.0		
68	0.0559	-0.5139	1.3371	1.4357	21.358	276.136	45.000	276.136	0.0	0.0		
69	0.0928	-0.5146	1.3371	1.4357	21.358	280.227	45.000	280.227	0.0	0.0		
70	0.1293	-0.5066	1.3371	1.4357	21.358	284.318	45.000	284.318	0.0	0.0		
71	0.1661	-0.4961	1.3371	1.4357	21.358	288.409	45.000	288.409	0.0	0.0		
72	0.2001	-0.4831	1.3371	1.4357	21.358	292.500	45.000	292.500	0.0	0.0		
73	0.2340	-0.4676	1.3371	1.4357	21.358	296.591	45.000	296.591	0.0	0.0		
74	0.2668	-0.4497	1.3371	1.4357	21.358	300.682	45.000	300.682	0.0	0.0		
75	0.2982	-0.4295	1.3371	1.4357	21.358	304.773	45.000	304.773	0.0	0.0		
76	0.3281	-0.4071	1.3371	1.4357	21.358	308.864	45.000	308.864	0.0	0.0		
77	0.3563	-0.3827	1.3371	1.4357	21.358	312.954	45.000	312.954	0.0	0.0		
78	0.3827	-0.3563	1.3371	1.4357	21.358	317.045	45.000	317.045	0.0	0.0		
79	0.4071	-0.3281	1.3371	1.4357	21.358	321.136	45.000	321.136	0.0	0.0		
80	0.4295	-0.2982	1.3371	1.4357	21.358	325.227	45.000	325.227	0.0	0.0		
81	0.4497	-0.2668	1.3371	1.4357	21.358	329.318	45.000	329.318	0.0	0.0		
82	0.4676	-0.2340	1.3371	1.4357	21.358	333.409	45.000	333.409	0.0	0.0		
83	0.4831	-0.2001	1.3371	1.4357	21.358	337.500	45.000	337.500	0.0	0.0		
84	0.4961	-0.1651	1.3371	1.4357	21.358	341.591	45.000	341.591	0.0	0.0		
85	0.5066	-0.1293	1.3371	1.4357	21.358	345.682	45.000	345.682	0.0	0.0		
86	0.5146	-0.0928	1.3371	1.4357	21.358	349.773	45.000	349.773	0.0	0.0		
87	0.5199	-0.0669	1.3371	1.4357	21.358	353.864	45.000	353.864	0.0	0.0		
88	0.5225	-0.0418	1.3371	1.4357	21.358	357.954	45.000	357.954	0.0	0.0		
89	0.5229	0.0	1.3158	22.473	0.0	0.0	45.000	0.0	0.0	0.0		
90	0.5229	0.0388	1.3158	22.473	1.4239	4.091	45.000	4.091	0.0	0.0		
91	0.5387	0.0775	1.3158	1.4239	1.4239	8.182	45.000	8.182	0.0	0.0		
92	0.5318	0.1157	1.3158	1.4239	1.4239	12.273	45.000	12.273	0.0	0.0		
93	0.5229	0.1533	1.3158	1.4239	1.4239	16.364	45.000	16.364	0.0	0.0		
94	0.5100	0.1902	1.3158	1.4239	1.4239	20.455	45.000	20.455	0.0	0.0		
95	0.4961	0.2261	1.3158	1.4239	1.4239	24.545	45.000	24.545	0.0	0.0		
96	0.4777	0.2608	1.3158	1.4239	1.4239	28.636	45.000	28.636	0.0	0.0		
97	0.4579	0.2943	1.3158	1.4239	1.4239	32.727	45.000	32.727	0.0	0.0		
98	0.4357	0.3262	1.3158	1.4239	1.4239	36.818	45.000	36.818	0.0	0.0		
99	0.4113	0.3564	1.3158	1.4239	1.4239	40.909	45.000	40.909	0.0	0.0		
100	0.3849	0.3849	1.3158	1.4239	1.4239	45.000	45.000	45.000	0.0	0.0		

Table 1 (Continued)

CUBE CORNER	CARTESIAN COORDINATES			SPHERICAL COORDINATES			DISTANCES-METERS			ANGLES-DEGREES			ORIENTATION ANGLES		
	X	Y	Z	R	THETA	PHI	C	PHI	C	THETA	PHI	N	THETA	PHI	N
101	0.3564	0.4113	1.3158	1.4239	22.473	49.091	45.000	49.091	45.000	45.000	49.091	45.000	45.000	49.091	0.0
102	0.3262	0.4357	1.3158	1.4239	22.473	51.182	45.000	51.182	45.000	45.000	51.182	45.000	45.000	51.182	0.0
103	0.2943	0.4579	1.3158	1.4239	22.473	57.273	45.000	57.273	45.000	45.000	57.273	45.000	45.000	57.273	0.0
104	0.2608	0.4777	1.3158	1.4239	22.473	61.364	45.000	61.364	45.000	45.000	61.364	45.000	45.000	61.364	0.0
105	0.2261	0.4951	1.3158	1.4239	22.473	65.455	45.000	65.455	45.000	45.000	65.455	45.000	45.000	65.455	0.0
106	0.1902	0.5100	1.3158	1.4239	22.473	69.545	45.000	69.545	45.000	45.000	69.545	45.000	45.000	69.545	0.0
107	0.1537	0.5222	1.3158	1.4239	22.473	73.636	45.000	73.636	45.000	45.000	73.636	45.000	45.000	73.636	0.0
108	0.1157	0.5318	1.3158	1.4239	22.473	77.727	45.000	77.727	45.000	45.000	77.727	45.000	45.000	77.727	0.0
109	0.0775	0.5387	1.3158	1.4239	22.473	81.818	45.000	81.818	45.000	45.000	81.818	45.000	45.000	81.818	0.0
110	0.0388	0.5429	1.3158	1.4239	22.473	85.909	45.000	85.909	45.000	45.000	85.909	45.000	45.000	85.909	0.0
111	-0.0000	0.5443	1.3158	1.4239	22.473	90.000	45.000	90.000	45.000	45.000	90.000	45.000	45.000	90.000	0.0
112	-0.0388	0.5429	1.3158	1.4239	22.473	94.091	45.000	94.091	45.000	45.000	94.091	45.000	45.000	94.091	0.0
113	-0.0775	0.5387	1.3158	1.4239	22.473	98.182	45.000	98.182	45.000	45.000	98.182	45.000	45.000	98.182	0.0
114	-0.1157	0.5318	1.3158	1.4239	22.473	102.273	45.000	102.273	45.000	45.000	102.273	45.000	45.000	102.273	0.0
115	-0.1537	0.5222	1.3158	1.4239	22.473	106.364	45.000	106.364	45.000	45.000	106.364	45.000	45.000	106.364	0.0
116	-0.1902	0.5100	1.3158	1.4239	22.473	110.455	45.000	110.455	45.000	45.000	110.455	45.000	45.000	110.455	0.0
117	-0.2261	0.4951	1.3158	1.4239	22.473	114.545	45.000	114.545	45.000	45.000	114.545	45.000	45.000	114.545	0.0
118	-0.2608	0.4777	1.3158	1.4239	22.473	118.636	45.000	118.636	45.000	45.000	118.636	45.000	45.000	118.636	0.0
119	-0.2943	0.4579	1.3158	1.4239	22.473	122.727	45.000	122.727	45.000	45.000	122.727	45.000	45.000	122.727	0.0
120	-0.3262	0.4357	1.3158	1.4239	22.473	126.818	45.000	126.818	45.000	45.000	126.818	45.000	45.000	126.818	0.0
121	-0.3564	0.4113	1.3158	1.4239	22.473	130.909	45.000	130.909	45.000	45.000	130.909	45.000	45.000	130.909	0.0
122	-0.3849	0.3849	1.3158	1.4239	22.473	135.000	45.000	135.000	45.000	45.000	135.000	45.000	45.000	135.000	0.0
123	-0.4113	0.3564	1.3158	1.4239	22.473	139.091	45.000	139.091	45.000	45.000	139.091	45.000	45.000	139.091	0.0
124	-0.4357	0.3262	1.3158	1.4239	22.473	143.182	45.000	143.182	45.000	45.000	143.182	45.000	45.000	143.182	0.0
125	-0.4579	0.2943	1.3158	1.4239	22.473	147.273	45.000	147.273	45.000	45.000	147.273	45.000	45.000	147.273	0.0
126	-0.4777	0.2608	1.3158	1.4239	22.473	151.364	45.000	151.364	45.000	45.000	151.364	45.000	45.000	151.364	0.0
127	-0.4951	0.2261	1.3158	1.4239	22.473	155.455	45.000	155.455	45.000	45.000	155.455	45.000	45.000	155.455	0.0
128	-0.5100	0.1902	1.3158	1.4239	22.473	159.545	45.000	159.545	45.000	45.000	159.545	45.000	45.000	159.545	0.0
129	-0.5222	0.1537	1.3158	1.4239	22.473	163.636	45.000	163.636	45.000	45.000	163.636	45.000	45.000	163.636	0.0
130	-0.5318	0.1157	1.3158	1.4239	22.473	167.727	45.000	167.727	45.000	45.000	167.727	45.000	45.000	167.727	0.0
131	-0.5387	0.0775	1.3158	1.4239	22.473	171.818	45.000	171.818	45.000	45.000	171.818	45.000	45.000	171.818	0.0
132	-0.5429	0.0388	1.3158	1.4239	22.473	175.909	45.000	175.909	45.000	45.000	175.909	45.000	45.000	175.909	0.0
133	-0.5443	-0.0000	1.3158	1.4239	22.473	180.000	45.000	180.000	45.000	45.000	180.000	45.000	45.000	180.000	0.0
134	-0.5429	-0.0388	1.3158	1.4239	22.473	184.091	45.000	184.091	45.000	45.000	184.091	45.000	45.000	184.091	0.0
135	-0.5387	-0.0775	1.3158	1.4239	22.473	188.182	45.000	188.182	45.000	45.000	188.182	45.000	45.000	188.182	0.0
136	-0.5318	-0.1157	1.3158	1.4239	22.473	192.273	45.000	192.273	45.000	45.000	192.273	45.000	45.000	192.273	0.0
137	-0.5222	-0.1537	1.3158	1.4239	22.473	196.364	45.000	196.364	45.000	45.000	196.364	45.000	45.000	196.364	0.0
138	-0.5100	-0.1902	1.3158	1.4239	22.473	200.455	45.000	200.455	45.000	45.000	200.455	45.000	45.000	200.455	0.0
139	-0.4951	-0.2261	1.3158	1.4239	22.473	204.545	45.000	204.545	45.000	45.000	204.545	45.000	45.000	204.545	0.0
140	-0.4777	-0.2608	1.3158	1.4239	22.473	208.636	45.000	208.636	45.000	45.000	208.636	45.000	45.000	208.636	0.0
141	-0.4579	-0.2943	1.3158	1.4239	22.473	212.727	45.000	212.727	45.000	45.000	212.727	45.000	45.000	212.727	0.0
142	-0.4357	-0.3262	1.3158	1.4239	22.473	216.818	45.000	216.818	45.000	45.000	216.818	45.000	45.000	216.818	0.0
143	-0.4113	-0.3564	1.3158	1.4239	22.473	220.909	45.000	220.909	45.000	45.000	220.909	45.000	45.000	220.909	0.0
144	-0.3849	-0.3849	1.3158	1.4239	22.473	225.000	45.000	225.000	45.000	45.000	225.000	45.000	45.000	225.000	0.0
145	-0.3564	-0.4113	1.3158	1.4239	22.473	229.091	45.000	229.091	45.000	45.000	229.091	45.000	45.000	229.091	0.0
146	-0.3262	-0.4357	1.3158	1.4239	22.473	233.182	45.000	233.182	45.000	45.000	233.182	45.000	45.000	233.182	0.0
147	-0.2943	-0.4579	1.3158	1.4239	22.473	237.273	45.000	237.273	45.000	45.000	237.273	45.000	45.000	237.273	0.0
148	-0.2608	-0.4777	1.3158	1.4239	22.473	241.364	45.000	241.364	45.000	45.000	241.364	45.000	45.000	241.364	0.0
149	-0.2261	-0.4951	1.3158	1.4239	22.473	245.455	45.000	245.455	45.000	45.000	245.455	45.000	45.000	245.455	0.0
150	-0.1902	-0.5100	1.3158	1.4239	22.473	249.545	45.000	249.545	45.000	45.000	249.545	45.000	45.000	249.545	0.0

Table 1 (Continued)

CUBE CORNER	CARTESIAN COORDINATES			SPHERICAL COORDINATES			DISTANCES-METERS			ANGLES-DEGREES			ORIENTATION ANGLES		
	X	Y	Z	R	THETA	PHI	C	PHI	DEGREES	THETA	DEGREES	PHI	THETA	PHI	GAMMA
151	0.1533	-0.5222	1.3158	1.4239	22.473	253.636	45.000	253.636	45.000	253.636	0.0	45.000	253.636	0.0	0.0
152	-0.1157	-0.5318	1.3158	1.4239	22.473	257.727	45.000	257.727	45.000	257.727	0.0	45.000	257.727	0.0	0.0
153	0.0775	-0.5387	1.3158	1.4239	22.473	261.818	45.000	261.818	45.000	261.818	0.0	45.000	261.818	0.0	0.0
154	-0.0368	-0.5423	1.3158	1.4239	22.473	265.909	45.000	265.909	45.000	265.909	0.0	45.000	265.909	0.0	0.0
155	0.0606	-0.5443	1.3158	1.4239	22.473	270.000	45.000	270.000	45.000	270.000	0.0	45.000	270.000	0.0	0.0
156	0.0368	-0.5429	1.3158	1.4239	22.473	274.091	45.000	274.091	45.000	274.091	0.0	45.000	274.091	0.0	0.0
157	0.0775	-0.5387	1.3158	1.4239	22.473	278.182	45.000	278.182	45.000	278.182	0.0	45.000	278.182	0.0	0.0
158	0.1157	-0.5318	1.3158	1.4239	22.473	282.273	45.000	282.273	45.000	282.273	0.0	45.000	282.273	0.0	0.0
159	0.1533	-0.5222	1.3158	1.4239	22.473	286.364	45.000	286.364	45.000	286.364	0.0	45.000	286.364	0.0	0.0
160	0.1902	-0.5100	1.3158	1.4239	22.473	290.454	45.000	290.454	45.000	290.454	0.0	45.000	290.454	0.0	0.0
161	0.2261	-0.4951	1.3158	1.4239	22.473	294.545	45.000	294.545	45.000	294.545	0.0	45.000	294.545	0.0	0.0
162	0.2608	-0.4777	1.3158	1.4239	22.473	298.636	45.000	298.636	45.000	298.636	0.0	45.000	298.636	0.0	0.0
163	0.2943	-0.4679	1.3158	1.4239	22.473	302.727	45.000	302.727	45.000	302.727	0.0	45.000	302.727	0.0	0.0
164	0.3262	-0.4357	1.3158	1.4239	22.473	306.818	45.000	306.818	45.000	306.818	0.0	45.000	306.818	0.0	0.0
165	0.3564	-0.4113	1.3158	1.4239	22.473	310.909	45.000	310.909	45.000	310.909	0.0	45.000	310.909	0.0	0.0
166	0.3849	-0.3849	1.3158	1.4239	22.473	315.000	45.000	315.000	45.000	315.000	0.0	45.000	315.000	0.0	0.0
167	0.4113	-0.3564	1.3158	1.4239	22.473	319.091	45.000	319.091	45.000	319.091	0.0	45.000	319.091	0.0	0.0
168	0.4357	-0.3262	1.3158	1.4239	22.473	323.182	45.000	323.182	45.000	323.182	0.0	45.000	323.182	0.0	0.0
169	0.4579	-0.2943	1.3158	1.4239	22.473	327.273	45.000	327.273	45.000	327.273	0.0	45.000	327.273	0.0	0.0
170	0.4777	-0.2608	1.3158	1.4239	22.473	331.364	45.000	331.364	45.000	331.364	0.0	45.000	331.364	0.0	0.0
171	0.4951	-0.2261	1.3158	1.4239	22.473	335.454	45.000	335.454	45.000	335.454	0.0	45.000	335.454	0.0	0.0
172	0.5100	-0.1902	1.3158	1.4239	22.473	339.545	45.000	339.545	45.000	339.545	0.0	45.000	339.545	0.0	0.0
173	0.5222	-0.1533	1.3158	1.4239	22.473	343.636	45.000	343.636	45.000	343.636	0.0	45.000	343.636	0.0	0.0
174	0.5318	-0.1157	1.3158	1.4239	22.473	347.727	45.000	347.727	45.000	347.727	0.0	45.000	347.727	0.0	0.0
175	0.5387	-0.0775	1.3158	1.4239	22.473	351.818	45.000	351.818	45.000	351.818	0.0	45.000	351.818	0.0	0.0
176	0.5429	-0.0368	1.3158	1.4239	22.473	355.909	45.000	355.909	45.000	355.909	0.0	45.000	355.909	0.0	0.0
177	0.5653	0.0202	1.2944	1.4126	23.605	2.045	45.000	2.045	45.000	2.045	0.0	45.000	2.045	0.0	0.0
178	0.5624	0.0605	1.2944	1.4126	23.605	6.136	45.000	6.136	45.000	6.136	0.0	45.000	6.136	0.0	0.0
179	0.5567	0.1064	1.2944	1.4126	23.605	10.227	45.000	10.227	45.000	10.227	0.0	45.000	10.227	0.0	0.0
180	0.5481	0.1399	1.2944	1.4126	23.605	14.318	45.000	14.318	45.000	14.318	0.0	45.000	14.318	0.0	0.0
181	0.5367	0.1786	1.2944	1.4126	23.605	18.409	45.000	18.409	45.000	18.409	0.0	45.000	18.409	0.0	0.0
182	0.5226	0.2165	1.2944	1.4126	23.605	22.500	45.000	22.500	45.000	22.500	0.0	45.000	22.500	0.0	0.0
183	0.5058	0.2532	1.2944	1.4126	23.605	26.591	45.000	26.591	45.000	26.591	0.0	45.000	26.591	0.0	0.0
184	0.4865	0.2886	1.2944	1.4126	23.605	30.682	45.000	30.682	45.000	30.682	0.0	45.000	30.682	0.0	0.0
185	0.4646	0.3226	1.2944	1.4126	23.605	34.773	45.000	34.773	45.000	34.773	0.0	45.000	34.773	0.0	0.0
186	0.4404	0.3549	1.2944	1.4126	23.605	38.864	45.000	38.864	45.000	38.864	0.0	45.000	38.864	0.0	0.0
187	0.4140	0.3854	1.2944	1.4126	23.605	42.955	45.000	42.955	45.000	42.955	0.0	45.000	42.955	0.0	0.0
188	0.3854	0.4140	1.2944	1.4126	23.605	47.045	45.000	47.045	45.000	47.045	0.0	45.000	47.045	0.0	0.0
189	0.3549	0.4404	1.2944	1.4126	23.605	51.136	45.000	51.136	45.000	51.136	0.0	45.000	51.136	0.0	0.0
190	0.3226	0.4680	1.2944	1.4126	23.605	55.227	45.000	55.227	45.000	55.227	0.0	45.000	55.227	0.0	0.0
191	0.2886	0.4865	1.2944	1.4126	23.605	59.318	45.000	59.318	45.000	59.318	0.0	45.000	59.318	0.0	0.0
192	0.2532	0.5058	1.2944	1.4126	23.605	63.409	45.000	63.409	45.000	63.409	0.0	45.000	63.409	0.0	0.0
193	0.2165	0.5226	1.2944	1.4126	23.605	67.500	45.000	67.500	45.000	67.500	0.0	45.000	67.500	0.0	0.0
194	0.1786	0.5367	1.2944	1.4126	23.605	71.591	45.000	71.591	45.000	71.591	0.0	45.000	71.591	0.0	0.0
195	0.1399	0.5481	1.2944	1.4126	23.605	75.682	45.000	75.682	45.000	75.682	0.0	45.000	75.682	0.0	0.0
196	0.1004	0.5567	1.2944	1.4126	23.605	79.773	45.000	79.773	45.000	79.773	0.0	45.000	79.773	0.0	0.0
197	0.0605	0.5624	1.2944	1.4126	23.605	83.864	45.000	83.864	45.000	83.864	0.0	45.000	83.864	0.0	0.0
198	0.0202	0.5653	1.2944	1.4126	23.605	87.955	45.000	87.955	45.000	87.955	0.0	45.000	87.955	0.0	0.0
199	-0.0202	0.5653	1.2944	1.4126	23.605	92.045	45.000	92.045	45.000	92.045	0.0	45.000	92.045	0.0	0.0
200	-0.0605	0.5624	1.2944	1.4126	23.605	96.136	45.000	96.136	45.000	96.136	0.0	45.000	96.136	0.0	0.0

Table 1 (Continued)

CUBE CORNER	CARTESIAN COORDINATES			DISTANCES-METERS			CUBE CORNER COORDINATES			SPHERICAL COORDINATES			ORIENTATION ANGLES		
	X	Y	Z	R	THETA	PHI	THETA	PHI	C	C	C	THETA	PHI	N	GAMMA
201	-0.1004	0.5567	1.2944	1.4126	23.605	100.227	45.000	100.227	100.227	100.227	45.000	100.227	100.227	100.227	0.0
202	-0.1189	0.5431	1.2944	1.4126	23.605	104.318	45.000	104.318	104.318	104.318	45.000	104.318	104.318	104.318	0.0
203	-0.1786	0.5367	1.2944	1.4126	23.605	108.409	45.000	108.409	108.409	108.409	45.000	108.409	108.409	108.409	0.0
204	-0.2165	0.5226	1.2944	1.4126	23.605	112.500	45.000	112.500	112.500	112.500	45.000	112.500	112.500	112.500	0.0
205	-0.2532	0.5058	1.2944	1.4126	23.605	116.591	45.000	116.591	116.591	116.591	45.000	116.591	116.591	116.591	0.0
206	-0.2886	0.4865	1.2944	1.4126	23.605	120.682	45.000	120.682	120.682	120.682	45.000	120.682	120.682	120.682	0.0
207	-0.3226	0.4646	1.2944	1.4126	23.605	124.773	45.000	124.773	124.773	124.773	45.000	124.773	124.773	124.773	0.0
208	-0.3549	0.4404	1.2944	1.4126	23.605	128.864	45.000	128.864	128.864	128.864	45.000	128.864	128.864	128.864	0.0
209	-0.3854	0.4140	1.2944	1.4126	23.605	132.955	45.000	132.955	132.955	132.955	45.000	132.955	132.955	132.955	0.0
210	-0.4140	0.3854	1.2944	1.4126	23.605	137.045	45.000	137.045	137.045	137.045	45.000	137.045	137.045	137.045	0.0
211	-0.4404	0.3549	1.2944	1.4126	23.605	141.136	45.000	141.136	141.136	141.136	45.000	141.136	141.136	141.136	0.0
212	-0.4646	0.3226	1.2944	1.4126	23.605	145.227	45.000	145.227	145.227	145.227	45.000	145.227	145.227	145.227	0.0
213	-0.4865	0.2886	1.2944	1.4126	23.605	149.318	45.000	149.318	149.318	149.318	45.000	149.318	149.318	149.318	0.0
214	-0.5058	0.2532	1.2944	1.4126	23.605	153.409	45.000	153.409	153.409	153.409	45.000	153.409	153.409	153.409	0.0
215	-0.5226	0.2165	1.2944	1.4126	23.605	157.500	45.000	157.500	157.500	157.500	45.000	157.500	157.500	157.500	0.0
216	-0.5367	0.1786	1.2944	1.4126	23.605	161.591	45.000	161.591	161.591	161.591	45.000	161.591	161.591	161.591	0.0
217	-0.5431	0.1399	1.2944	1.4126	23.605	165.682	45.000	165.682	165.682	165.682	45.000	165.682	165.682	165.682	0.0
218	-0.5567	0.1004	1.2944	1.4126	23.605	169.773	45.000	169.773	169.773	169.773	45.000	169.773	169.773	169.773	0.0
219	-0.5624	0.0605	1.2944	1.4126	23.605	173.864	45.000	173.864	173.864	173.864	45.000	173.864	173.864	173.864	0.0
220	-0.5653	0.0202	1.2944	1.4126	23.605	177.955	45.000	177.955	177.955	177.955	45.000	177.955	177.955	177.955	0.0
221	-0.5653	-0.0202	1.2944	1.4126	23.605	182.045	45.000	182.045	182.045	182.045	45.000	182.045	182.045	182.045	0.0
222	-0.5624	-0.0605	1.2944	1.4126	23.605	186.136	45.000	186.136	186.136	186.136	45.000	186.136	186.136	186.136	0.0
223	-0.5567	-0.1004	1.2944	1.4126	23.605	190.227	45.000	190.227	190.227	190.227	45.000	190.227	190.227	190.227	0.0
224	-0.5431	-0.1399	1.2944	1.4126	23.605	194.318	45.000	194.318	194.318	194.318	45.000	194.318	194.318	194.318	0.0
225	-0.5226	-0.1786	1.2944	1.4126	23.605	198.409	45.000	198.409	198.409	198.409	45.000	198.409	198.409	198.409	0.0
226	-0.5058	-0.2165	1.2944	1.4126	23.605	202.500	45.000	202.500	202.500	202.500	45.000	202.500	202.500	202.500	0.0
227	-0.4865	-0.2532	1.2944	1.4126	23.605	206.591	45.000	206.591	206.591	206.591	45.000	206.591	206.591	206.591	0.0
228	-0.4646	-0.2886	1.2944	1.4126	23.605	210.682	45.000	210.682	210.682	210.682	45.000	210.682	210.682	210.682	0.0
229	-0.4404	-0.3226	1.2944	1.4126	23.605	214.773	45.000	214.773	214.773	214.773	45.000	214.773	214.773	214.773	0.0
230	-0.4140	-0.3549	1.2944	1.4126	23.605	218.864	45.000	218.864	218.864	218.864	45.000	218.864	218.864	218.864	0.0
231	-0.3854	-0.3854	1.2944	1.4126	23.605	222.955	45.000	222.955	222.955	222.955	45.000	222.955	222.955	222.955	0.0
232	-0.3549	-0.4140	1.2944	1.4126	23.605	227.045	45.000	227.045	227.045	227.045	45.000	227.045	227.045	227.045	0.0
233	-0.3226	-0.4404	1.2944	1.4126	23.605	231.136	45.000	231.136	231.136	231.136	45.000	231.136	231.136	231.136	0.0
234	-0.2886	-0.4646	1.2944	1.4126	23.605	235.227	45.000	235.227	235.227	235.227	45.000	235.227	235.227	235.227	0.0
235	-0.2532	-0.4865	1.2944	1.4126	23.605	239.318	45.000	239.318	239.318	239.318	45.000	239.318	239.318	239.318	0.0
236	-0.2165	-0.5058	1.2944	1.4126	23.605	243.409	45.000	243.409	243.409	243.409	45.000	243.409	243.409	243.409	0.0
237	-0.1786	-0.5226	1.2944	1.4126	23.605	247.500	45.000	247.500	247.500	247.500	45.000	247.500	247.500	247.500	0.0
238	-0.1399	-0.5367	1.2944	1.4126	23.605	251.591	45.000	251.591	251.591	251.591	45.000	251.591	251.591	251.591	0.0
239	-0.1004	-0.5431	1.2944	1.4126	23.605	255.682	45.000	255.682	255.682	255.682	45.000	255.682	255.682	255.682	0.0
240	-0.0605	-0.5567	1.2944	1.4126	23.605	259.773	45.000	259.773	259.773	259.773	45.000	259.773	259.773	259.773	0.0
241	-0.0202	-0.5624	1.2944	1.4126	23.605	263.864	45.000	263.864	263.864	263.864	45.000	263.864	263.864	263.864	0.0
242	0.0202	-0.5653	1.2944	1.4126	23.605	267.955	45.000	267.955	267.955	267.955	45.000	267.955	267.955	267.955	0.0
243	0.0605	-0.5653	1.2944	1.4126	23.605	272.045	45.000	272.045	272.045	272.045	45.000	272.045	272.045	272.045	0.0
244	0.1004	-0.5624	1.2944	1.4126	23.605	276.136	45.000	276.136	276.136	276.136	45.000	276.136	276.136	276.136	0.0
245	0.1399	-0.5567	1.2944	1.4126	23.605	280.227	45.000	280.227	280.227	280.227	45.000	280.227	280.227	280.227	0.0
246	0.1786	-0.5431	1.2944	1.4126	23.605	284.318	45.000	284.318	284.318	284.318	45.000	284.318	284.318	284.318	0.0
247	0.2165	-0.5226	1.2944	1.4126	23.605	288.409	45.000	288.409	288.409	288.409	45.000	288.409	288.409	288.409	0.0
248	0.2532	-0.5058	1.2944	1.4126	23.605	292.500	45.000	292.500	292.500	292.500	45.000	292.500	292.500	292.500	0.0
249	0.2886	-0.4865	1.2944	1.4126	23.605	296.591	45.000	296.591	296.591	296.591	45.000	296.591	296.591	296.591	0.0
250	0.3226	-0.4646	1.2944	1.4126	23.605	300.682	45.000	300.682	300.682	300.682	45.000	300.682	300.682	300.682	0.0

Table 1 (Continued)

CUBE CURNER	CARTESIAN COORDINATES			SPHERICAL COORDINATES			DISTANCES-METERS			ANGLES-DEGREES		
	X	Y	Z	R	THETA	PHI	R	THETA	PHI	THETA	PHI	GAMMA
251	0.3226	-0.4646	1.2944	1.4126	23.605	304.773	1.4126	23.605	304.773	45.000	304.773	0.0
252	0.3549	-0.4404	1.2944	1.4126	23.605	308.864	1.4126	23.605	308.864	45.000	308.864	0.0
253	0.3854	-0.4140	1.2944	1.4126	23.605	312.954	1.4126	23.605	312.954	45.000	312.954	0.0
254	0.4140	-0.3854	1.2944	1.4126	23.605	317.045	1.4126	23.605	317.045	45.000	317.045	0.0
255	0.4404	-0.3549	1.2944	1.4126	23.605	321.136	1.4126	23.605	321.136	45.000	321.136	0.0
256	0.4646	-0.3226	1.2944	1.4126	23.605	325.227	1.4126	23.605	325.227	45.000	325.227	0.0
257	0.4865	-0.2886	1.2944	1.4126	23.605	329.318	1.4126	23.605	329.318	45.000	329.318	0.0
258	0.5058	-0.2532	1.2944	1.4126	23.605	333.409	1.4126	23.605	333.409	45.000	333.409	0.0
259	0.5226	-0.2165	1.2944	1.4126	23.605	337.500	1.4126	23.605	337.500	45.000	337.500	0.0
260	0.5367	-0.1786	1.2944	1.4126	23.605	341.591	1.4126	23.605	341.591	45.000	341.591	0.0
261	0.5481	-0.1399	1.2944	1.4126	23.605	345.682	1.4126	23.605	345.682	45.000	345.682	0.0
262	0.5567	-0.1004	1.2944	1.4126	23.605	349.773	1.4126	23.605	349.773	45.000	349.773	0.0
263	0.5624	-0.0605	1.2944	1.4126	23.605	353.864	1.4126	23.605	353.864	45.000	353.864	0.0
264	0.5653	-0.0202	1.2944	1.4126	23.605	357.954	1.4126	23.605	357.954	45.000	357.954	0.0

SATELLITE CROSS SECTION

Definition of Terms

The number of photons received from a retroreflector array by a laser ranging system is obtained by the following relation:

$$N = \frac{1}{2\pi} \frac{\eta E_T D_R^2 \gamma_A^2 \rho_o \sigma}{(h\nu) \theta_T^2 R^4}$$

where

- N = number of photons received
- η = quantum efficiency of receiver phototube
- E_T = energy of transmitted pulse
- D_R = diameter of receiver optics
- γ_A = transmission of atmosphere
- ρ_o = optical efficiency of transmitter and receiver
- σ = radar cross section of the target
- $h\nu$ = energy of a photon
- θ_T = transmitted beam divergence
- R = range to the target

The derivation of this equation is shown in Appendix B. Of all these terms only one (σ) is a parameter of the targets. Radar cross section defines the effectiveness of the array from a ranging standpoint, and therefore, one purpose of these tests was to determine the cross section, which is defined as:

$$\sigma = \rho AG$$

where ρ is the optical efficiency, A, the reflective area, and G, the gain of the array. Gain, in turn, is defined as the intensity of the reflected radiation in the desired direction divided by the intensity that would have occurred if the reflected energy had been uniformly distributed over 4π steradians.

In general, the cross section is a function of the aspect angle of the laser beam with respect to the array, and the position of the receiver in the far-field pattern of the array. Since the Geos-3 array is rotationally symmetric about the Z axis, the laser incidence angle can be defined by one angle (θ_L) measured with respect to the Z axis.

Due to the motion of the satellite in orbit, an effect known as the velocity aberration causes the reflected radiation from the satellite to be displaced angularly from the transmitter/satellite axis. For the Geos-3 satellite at an altitude of 843 km, this displacement amounts to $49.6 \mu\text{r}$, and therefore cross section must be measured at this angle. If we define a polar coordinate system about the satellite transmitter axis, in general, the far-field pattern will

have minor variations in azimuth as well as the major variations with polar angle. These minor variations with azimuth have not been taken into account in this analysis except through a listing of the maximum and minimum values that occur at different azimuths.

Theoretical Analysis

An analysis of the cross section as a function of laser incidence angle for a velocity aberration of $49.6 \mu r$ was performed at a wavelength of 6943 \AA using the RETRO program which calculates the performance of laser retroreflector arrays. Results are shown in figure 4 and table 2. Due to the design of the cube corners, these results are applicable for any wavelength in the 4000- to 7000-\AA visible range with only minor changes. To convert the data to other wavelengths, the following equation should be used.

$$\sigma_{\lambda} = \sigma_{6943} \frac{(6.943 \times 10^{-7})^2}{\lambda^2}$$

where λ is in meters.

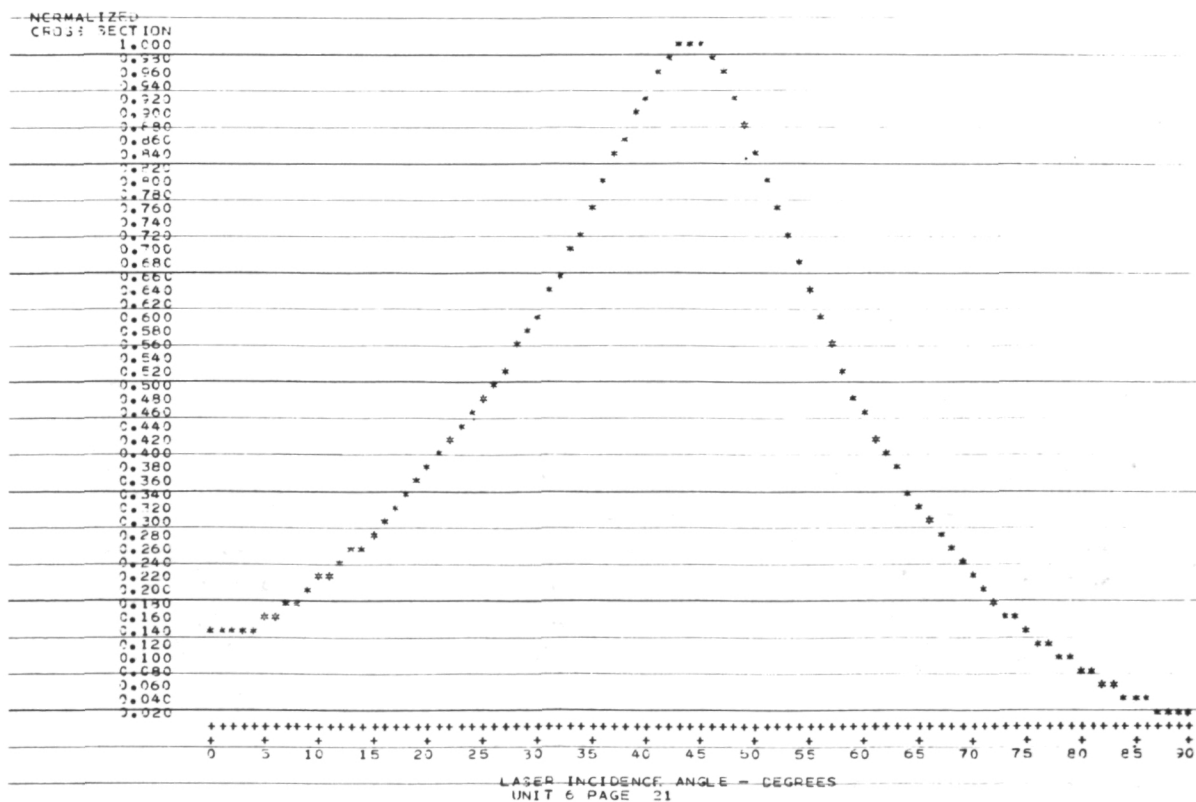


Figure 4. Normalized cross section versus incidence angle.

Table 2
Cross Section versus Incidence Angle

INCIDENCE ANGLE	CROSS SECTION	INCIDENCE ANGLE	CROSS SECTION	INCIDENCE ANGLE	CROSS SECTION
(DEGREES)	(METERS ² x 10 ⁶)	(DEGREES)	(METERS ² x 10 ⁶)	(DEGREES)	(METERS ² x 10 ⁶)
0	2.9327	31	14.1625	61	9.4663
1	2.9512	32	14.8005	62	8.8439
2	3.0067	33	15.4422	63	8.2511
3	3.1093	34	16.1614	64	7.6896
4	3.2550	35	16.9404	65	7.1667
5	3.4378	36	17.7421	66	6.6887
6	3.6550	37	18.5410	67	6.2239
7	3.9055	38	19.3074	68	5.7757
8	4.1885	39	20.0366	69	5.3417
9	4.4641	40	20.7066	70	4.9218
10	4.7374	41	21.3070	71	4.5192
11	5.0104	42	21.7753	72	4.1399
12	5.3046	43	22.1026	73	3.7766
13	5.6075	44	22.2734	74	3.4353
14	5.9479	45	22.2340	75	3.1129
15	6.3185	46	21.8719	76	2.8152
16	6.7119	47	21.3133	77	2.5418
17	7.1238	48	20.6194	78	2.2943
18	7.5502	49	19.8084	79	2.0576
19	7.9866	50	18.8931	80	1.8337
20	8.4350	51	17.9429	81	1.6186
21	8.8937	52	16.9752	82	1.4112
22	9.3532	53	15.9857	83	1.2085
23	9.8149	54	15.0056	84	1.0268
24	10.2787	55	14.0551	85	0.8654
25	10.7420	56	13.1418	86	0.7214
26	11.2495	57	12.3038	87	0.5961
27	11.7905	58	11.5554	88	0.4882
28	12.3524	59	10.8249	89	0.3938
29	12.9281	60	10.1294	90	0.3137
30	13.5337				

Experimental Apparatus and Procedure

Optical Systems

The optical system used in these tests is shown in figure 5. A helium neon laser was passed through the spatial filter and beam expander to generate a 50-mm diameter collimated laser beam. This radiation then passed through a beam splitter to a second objective which focused the beam at the focus of an 86-cm diameter f/9.31 aluminized parabola. A small aluminized flat was used near the focus of the parabola to fold the system. The output of this system was a highly collimated 86-cm diameter laser beam. One quarter (2 panels) of the Geos-3 array was mounted on a rotating platform in such a manner that the array was fully illuminated, and could be rotated by 90 degrees around an axis perpendicular to the symmetry axis of the full array. Although only one quarter of the array was used, the resulting far-field patterns were the same (except for intensity) as those from the full array, due to symmetry. Because of the array geometry, only half of the array is active at one time (except for within 5 degrees of the symmetry axis). Therefore, the results of the tests must be scaled by 2 to obtain the final result except for near-zero incidence angles where the scale factor was 4. Tests were performed at 5-degree increments of incidence angle from 0 degrees to 60 degrees and therefore the scale factor of 4 was applied only to the 0-degree result.

Reflected radiation returned to the parabola and back through the system to the beam-splitter where about half of the radiation was directed into a 0.91-m focal length collimator.

The effective focal length of the system in the reflected mode was

$$f = 0.91 \times \frac{81.57}{0.45} = 16.5 \text{ m}$$

Since a 100-m focal length was desired, the image was magnified by a microscope objective to obtain the proper image scale.

The flat shown mounted behind the array served two functions—scale calibration and cross-section calibration. The flat was exposed to the collimated beam by removing the array, and was aligned to produce an image at the same position as the center of the pattern from the array. A mask was then placed over the flat containing a double slit with a spacing of 63.28 mm. This produced a Young's interference pattern in the far field with a spacing of $10 \mu\text{m}$ per cycle. Since the desired focal length was 100 m, focal length calibration was accomplished by adjusting the microscope objective until a focused image with a spacing between fringes of 1 mm was accomplished. Since about 30 fringes were visible and measurement of the fringes could be made to about $\pm 1/4$ fringe, the net accuracy in determining image scale was approximately 1 percent.

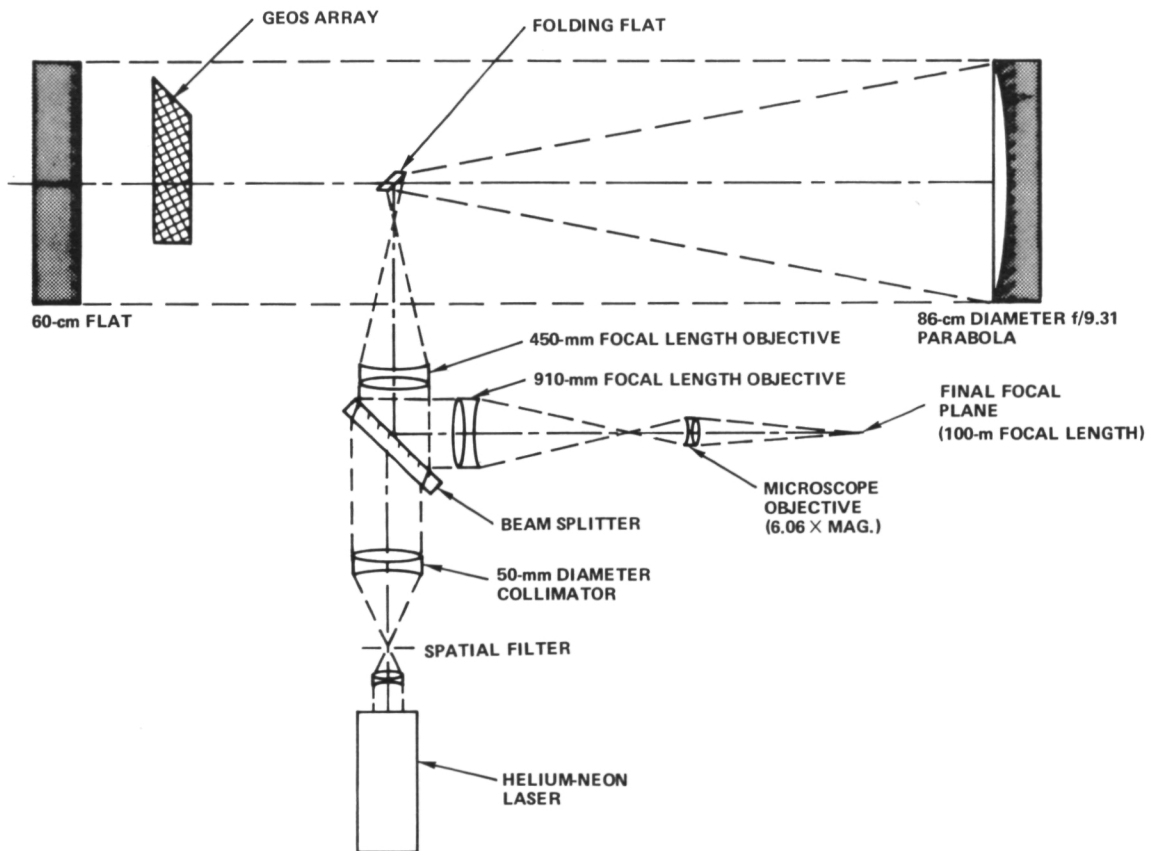


Figure 5. Optical system for cross-section tests.

Conversion of intensity in the focal plane into units of cross section was accomplished by measuring the intensity from a circular aperture in a mask covering the flat. Since the cross section for a flat is

$$\sigma = \frac{4\pi A^2}{\lambda^2} \rho$$

where A is the area of the flat, λ is wavelength, and ρ is the optical efficiency, the area of the aperture could be calculated, and from this, the intensities in the focal plane related to cross section. An optical efficiency of 91 percent was used for the flat to account for the reflection loss.

Image Scanner

A tape-driven mechanical scanner was used to scan the final image plane. This scanner supported a photomultiplier with a helium-neon filter and a small pinhole. The system was constructed so that the pinhole was accurately in the focal plane and only light going through the pinhole could reach the photomultiplier. The scanner covered a 25- by 25-mm area in 25 lines spaced 1 mm apart. The scan was performed in a zig-zag manner, traversing from left to right, stepping down 1mm, traversing from right to left, etc., until the area was covered. Since the scale was 10 μ r per mm, this provided 25 scans at 10- μ r increments. The pinhole was approximately 0.25 mm in diameter (or 2.5 μ r in angular width).

Image Scanner Readout

Potentiometers were attached to the scanner to read out image position. The photomultiplier output and the potentiometer outputs were simultaneously recorded on a four-channel chart recorder as the scan proceeded. A sample chart recording is shown in figure 6. A photograph of the pattern is shown in figure 7. On the top of figure 6, in track #1, the intensity (cross section) as a function of time is shown. The second track shows the vertical position of the scanner. The scale of the chart recording is twice the image scale, so that each line increment appears as a 2-mm displacement. The bottom track shows the horizontal position of the pinhole. Where the line is sloping upward from left to right, the scan was from left to right, while where it slopes downward, the scan is from right to left. The flat section at the top and bottom of this track are the times when the scanner is stepping from one line to the next. A theoretical calculation of the image profile can be seen in figure 8. The data shown in figures 6 and 7 were taken for a reference array consisting of 69, 15-mm hexagonal diffraction-limited cube corners of the Navigational Technology Satellite (NTS-1) type. The peak cross section is $70.5 \times 10^6 \text{ m}^2$ for this array.

Summary of Satellite Cross-Section Measurements

The image scanner readouts are shown in detail in Appendix C. A sample scan across the center of the far-field diffraction pattern for an incidence angle of 45° is shown in figure 9. Due to the dihedral spoiling built into the cube corners, the far-field diffraction has a toroidal which,

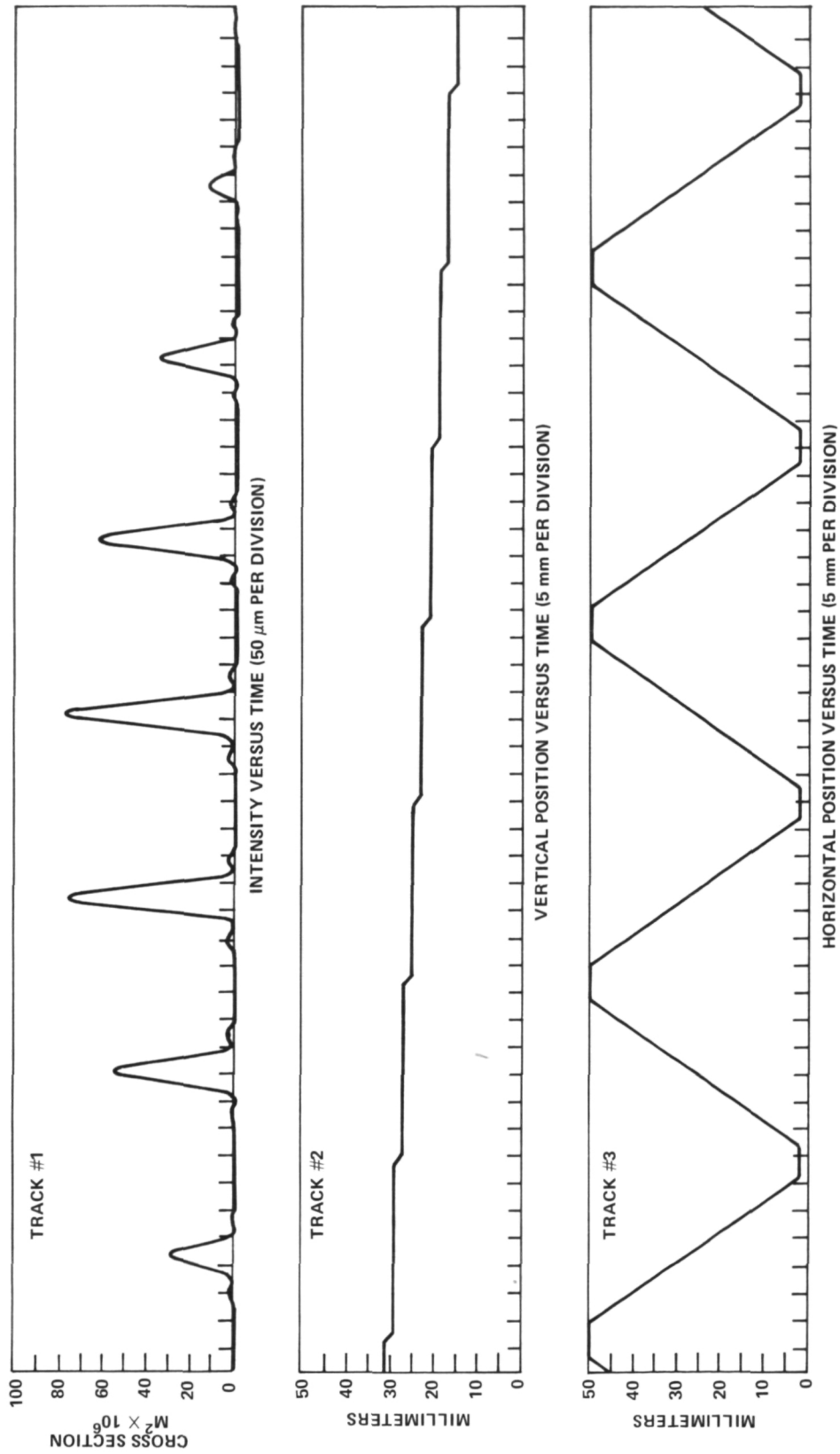


Figure 6. Phototube output.

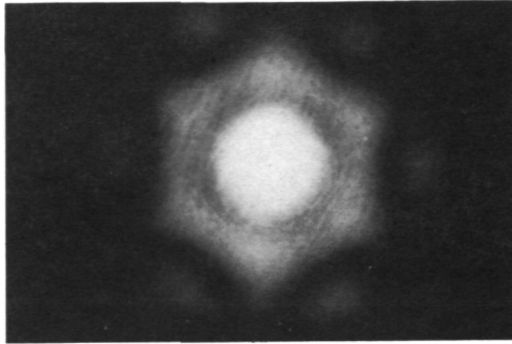


Figure 7. Far-field pattern photograph.

when shown in profile, appears as two peaks occurring at $\pm 50 \mu\text{r}$ from the retrodirected direction. This splitting places the maximum cross section at the velocity aberration angle and maximizes the signal for the given size and number of cube corners.

An analysis of the image plane scans gives the cross section as a function of incidence angle at $49.6 \mu\text{r}$ off-axis as shown in table 3 and figure 10. The maximum and minimum values found in a circle in the far-field diffraction pattern (FEDP) with a radius of $49.6 \mu\text{r}$ are shown in figure 10 by the vertical bars. Values calculated with the RETRO program are shown by open circles. While the experimental and calculated curves show the same general shape, there is an obvious difference in their absolute magnitude. Except for incidence angles less than 20 degrees, the experimental values tend to be 50 to 70 percent higher than the calculated values. Because the experimental values were measured at 6328 \AA , diffraction

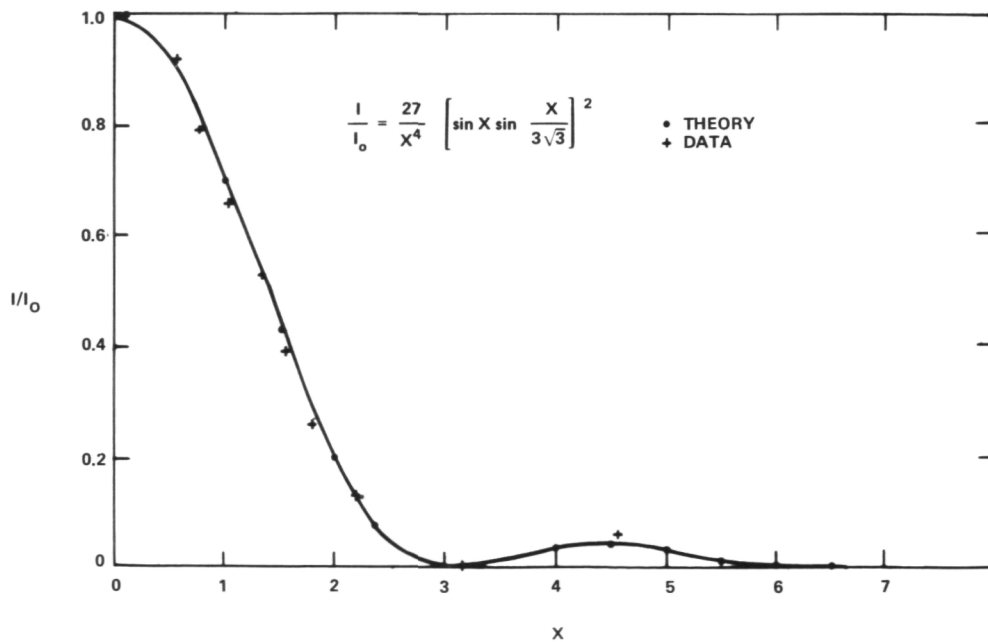


Figure 8. Comparison of measured and computed far-field patterns.

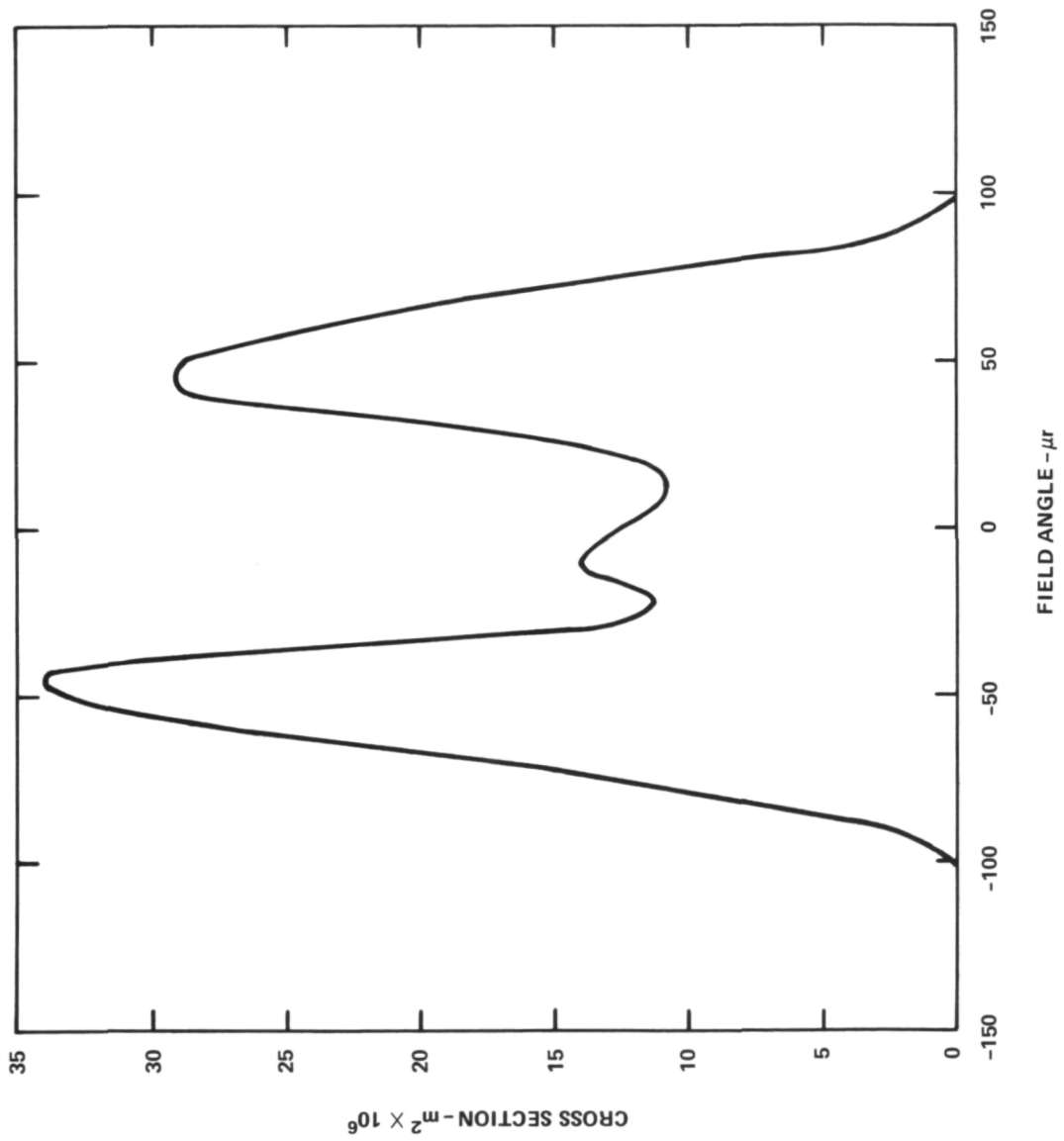


Figure 9. Far-field profile for 45° incidence.

Table 3
 Cross Section versus Incidence Angle - Geos-3

Incidence Angle (Degrees)	Cross Section - Meters ² × 10 ⁶	
	Measured (6328 Å) Min – Max	Calculated (6943 Å)
0	1.9 – 1.9	3.0
10	1.9 – 5.6	4.7
20	9.3 – 19	8.4
30	19 – 30	14.0
40	24 – 46	21.0
45	28 – 46	22.0
50	28 – 37	19.0
60	9.3 – 19	10.0
70	– –	4.9

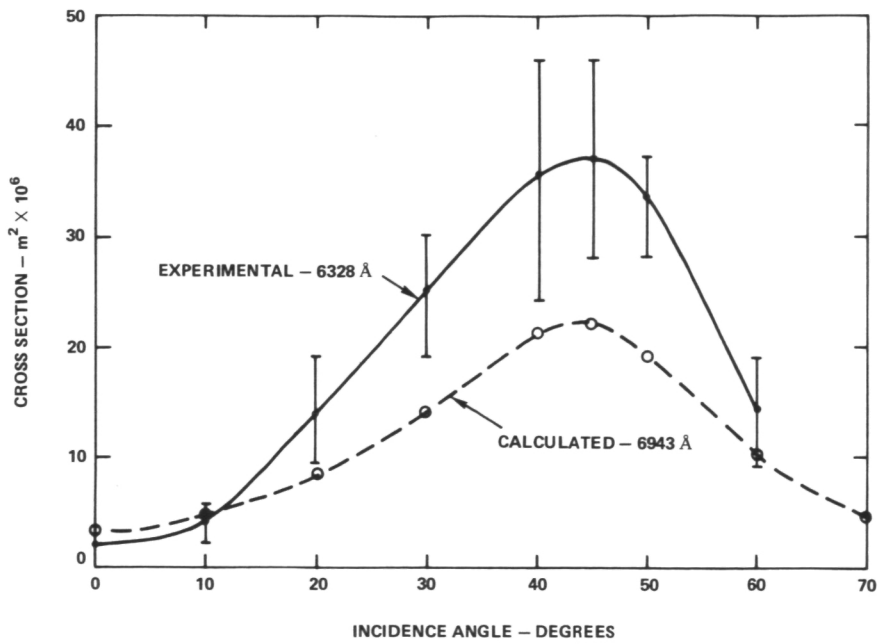


Figure 10. Cross section versus incidence angle.

could cause as much as a 20-percent increase, but this does not account for all of the observed differences. The remainder can be accounted for by the fact that the calculations were performed for the case of satellite velocity normal to the incident radiation, which causes the maximum velocity aberration and minimum effective cross section. Therefore close agreement between the minimum experimental and wavelength-corrected calculated values would be expected. In table 4 and figure 11, calculated cross sections have been increased by 20.4 percent to account for the wavelength difference and are compared to the minimum experimental values. As expected, the agreement is very good so that one curve can reasonably represent both experimental and calculated values. The measured values of cross section in table 3 and figure 10, therefore, are in close agreement with the expected values, and are the values which should be used in all range equation solutions. The difference between the maximum and minimum cross-section values is due to the asymmetry caused by diffraction. For operation at wavelengths other than 6328 Å, the cross section should be multiplied by the following factor if maximum precision is required (λ in Angstroms). However, such accuracy

$$F = \left[\frac{6328}{\lambda} \right]^2$$

is seldom needed in calculations of signal strength.

Table 4
Comparison of Wavelength Adjusted and Experimental Cross
Section versus Incidence Angle - Geos-3

Incidence Angle (Degrees)	Cross Section - Meters ² × 10 ⁶	
	Measured (6328 Å)	Calculated* (6328 Å)
0	1.9	3.6
10	1.9	5.6
20	9.3	11
30	19	17
40	24	25
45	28	26
50	28	23
60	9.3	12
70	—	5.9

*Increased by 20.4 percent from values of table 3 to account for diffraction effects.

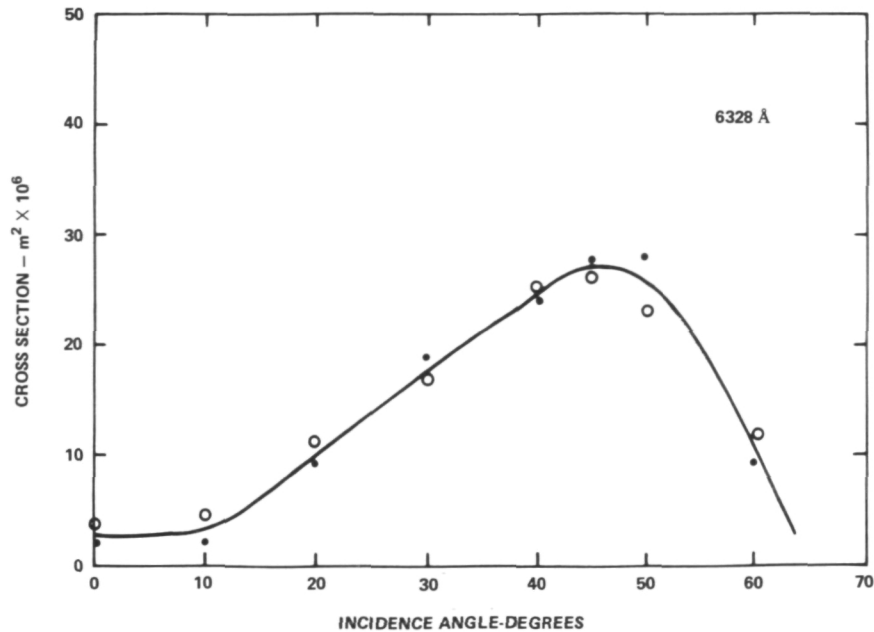


Figure 11. Comparison of wavelength adjusted calculated and experimental cross section versus incidence angle.

TARGET SIGNATURE TESTS

In these tests, the satellite array was evaluated in terms of the amount of temporal spreading and distortion imposed on a subnanosecond pulse, and the value and attitude dependence of the range correction. The instrumentation system and the tests' results are described in the following sections.

Optical System

The optical system used in these tests is shown schematically in figure 12. A Nd: YAG* laser with an external pulse selector furnished a 10-kHz pulse train at $0.53 \mu\text{m}$. Each pulse had a width of about 140 ps (FWHM) and an energy of about 10^{-12} joules. This beam was spatially filtered and recollimated at 50-mm diameter using a Spectra-Physics #331/332 telescope. This beam was sent through a 45-45 beam splitter (used for transmitter-receiver isolation) and brought to a focus within a few millimeters of the front surface of the folding flat. This image plane was located precisely at the prime focus of the large (86-cm) parabola, so that after passing through focus, the beam expanded, filled the parabola, and was recollimated. This collimated beam then illuminated either the 60-cm reference flat (used for alignment and calibration) or the satellite and reference arrays. The return signal traverses the exact same path due to the retrodirective property of cube corners, and is separated from the transmitted signal by the beam splitter.

*Nd: YAG = neodymium yttrium aluminum garnet.

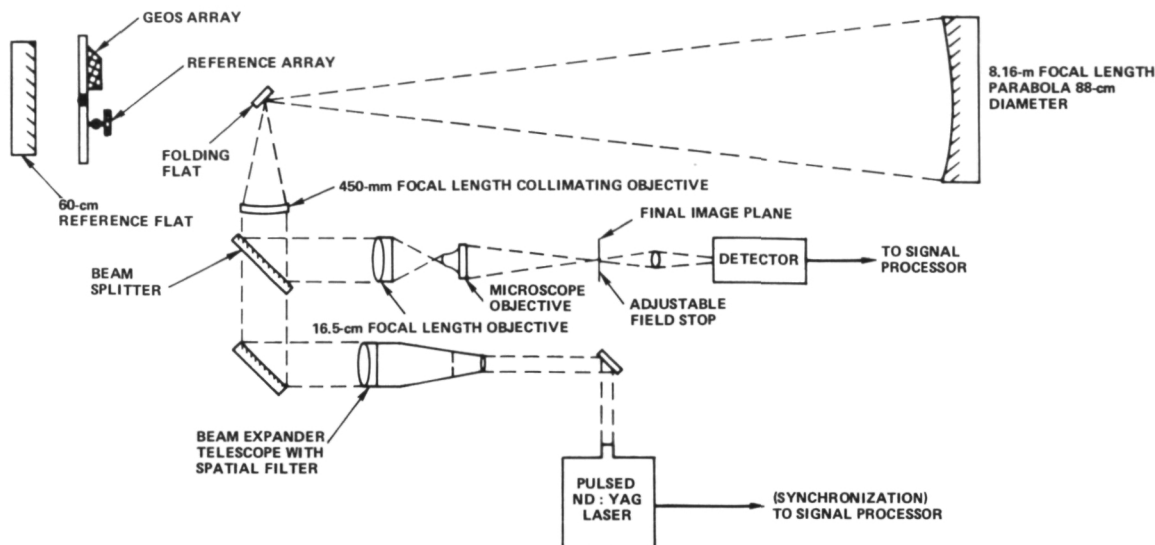


Figure 12. Optical system for target signature tests.

The combination of the 16.5-cm f.1 objective and the microscope objective controls the receiver system focal plane scaling; in these tests, an equivalent focal length of 30 m was maintained in the final image plane. This resulted in an image plane scaling of 33.3 microradians per millimeter. Two sizes of field stops were used during these tests; when the full far-field pattern was being detected, a stop of 3.25-mm diameter ($108 \mu\text{r}$) was installed; when a point in the far field was being measured, a stop of 0.41-mm diameter ($13.7 \mu\text{r}$) was used. The energy passing through the field stop was collected by a simple lens and focused onto the photocathode of the detector. The field stop, lens, and detector were mounted on a common base that had 2-axis linear motion with precision better than 0.01 mm. Mounting these pieces on a common base ensured that the same portion of the photocathode was illuminated throughout the tests, thereby obviating concern about position-dependent biases induced by the detector. The electrical signal from the detector, as well as a synchronization signal from the laser were sent to the signal processor. The satellite array and a reference flat array were attached to a common mount with vertical axes of rotation as shown in figure 12. A picture of these two units as mounted is shown in figure 13, and a picture of the overall optical system is shown in figure 14. For the pulse distortion tests, each pulse sent out by the laser resulted in two received pulses; one pulse is reflected by the flat reference array, and the second is reflected by the satellite array.

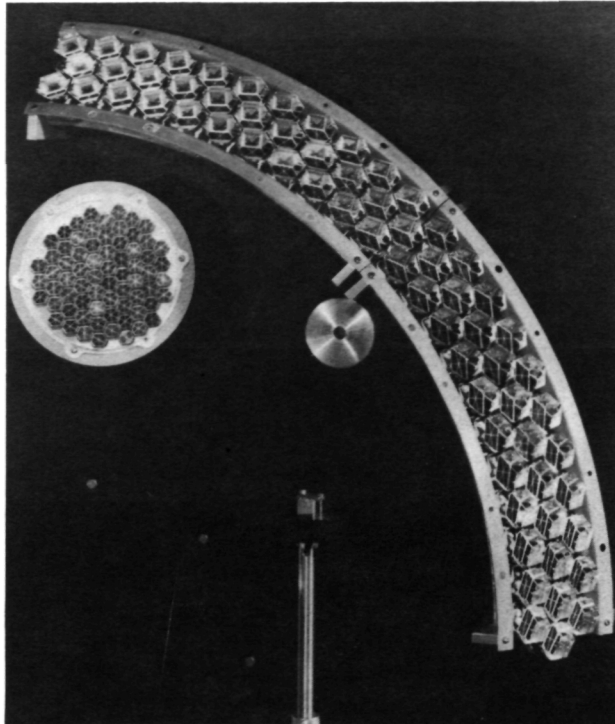


Figure 13. Mounting configuration for Geos and reference arrays.

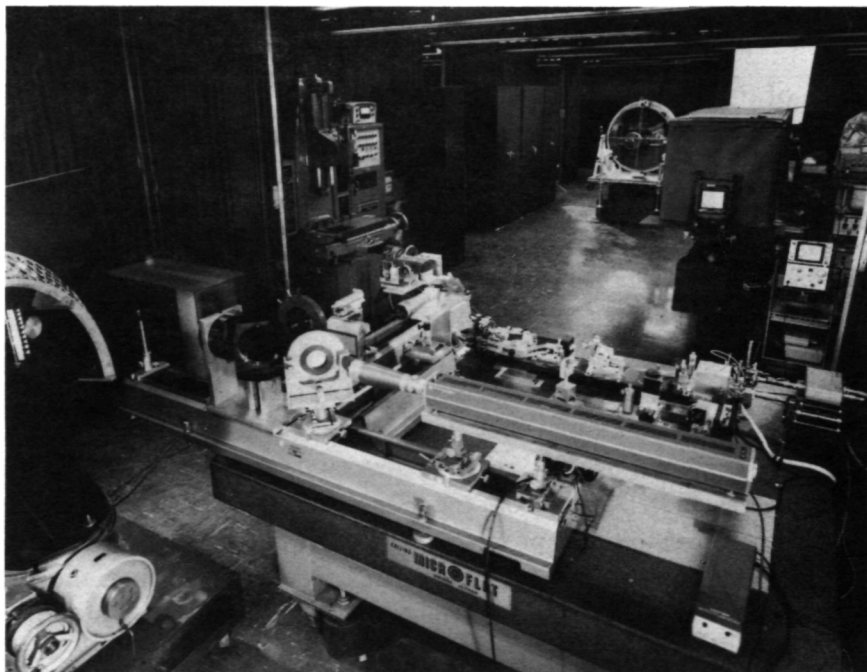


Figure 14. Overview of target signature test set-up.

The reference array is flat and is in all cases aligned normal to the incident beam. It induces zero temporal spreading, therefore the detection of this pulse gives a direct reading of the bandwidth and resolution of the entire system. The satellite array pulse that is detected is compared to the reference pulse, and any differences in shape are attributed to the satellite array, since all other elements in the system are common to both pulses. Waveform measurements were made at Geos array orientations from 0 to 65 degrees, with the reference array adjusted for normal incidence at each Geos array setting. Range correction measurements were made in a similar way, but the information of interest in this case is the relative position (in time) of the two reflected pulses. Knowing the properties of the cube corners in the reference array, the point in space from which the reference pulses are reflected can be defined precisely. By physically measuring the location of reference and satellite arrays, and knowing the measured location of the satellite center of mass with respect to mounting points on the Geos array, the range correction can be evaluated for any array (that is, satellite) orientation.

Laser Transmitter

The details of the laser subsystem used in these tests are shown in figure 15. A continuous wave (cw) pumped Nd: YAG laser is mode locked using an acousto-optic loss modulator. With the modulator driven at 200 MHz, the 1.06- μm output pulse train occurs at a 400 MHz rate and has an average power of about 0.1 W.

This beam is brought to a focus in a 5-mm cube of barium sodium niobate which converts about 1 percent of the incident power into the second harmonic frequency, which is at a wavelength of 0.53 μm . All target signature tests were conducted at this wavelength, with the fundamental wavelength being used only for monitoring laser amplitude and pulse stability. The fundamental and second harmonic frequencies are separated by a dichroic beam splitter and the 0.53- μ pulse train was directed into a high speed electro-optic shutter. This unit had a rise time of about 1 ns and was therefore able to select single pulses for transmission, while blocking adjacent pulses (with an extinction ratio of about 20:1). The electrical trigger signal for the gate was derived from the 200-MHz drive to the mode locker; synchronization between the synthesizer signal, the counted down gate trigger, and the optical pulses was maintained to better than 50 ps throughout the testing.

The high speed shutter was required in these tests for two reasons. First, the basic interpulse spacing of the laser was 2.5 ns, and this was uncomfortably close to the width of the composite waveform from the Geos and reference arrays. If the received waveform was allowed to repeat on a 2.5-ns period, system resolution would have been degraded due to interpulse effects. Secondly, the maximum average current capability of the receiver detector would have been exceeded with signal levels of about 15 photoelectrons per pulse, if the input rate were 4×10^8 per second.

So the inclusion of the gate permitted higher resolution in the wave-form analysis and also permitted operation at large optical signal-to-noise ratios (SNR).

Multialkali 6-Stage Static Crossed Field Photomultiplier (Continued)
(Varian #153A)

Bandwidth, 0 to -3 dB	DC to 2.5 GHz
Anode Rise Time (10% to 90%)	150 ps
Output Coupler	50 ohm coaxial OSM
Dimensions, housed with magnets	8.3 cm X 6.7 cm X 15.9 cm long (3-1/4 in.) X (2-5/8 in.) X (6-1/4 in.) long
Weight	1.8 kg (4 lbs.)
Operating Voltages	Photocathode: -2900 Vdc typ. Rail: + 950 Vdc typ.

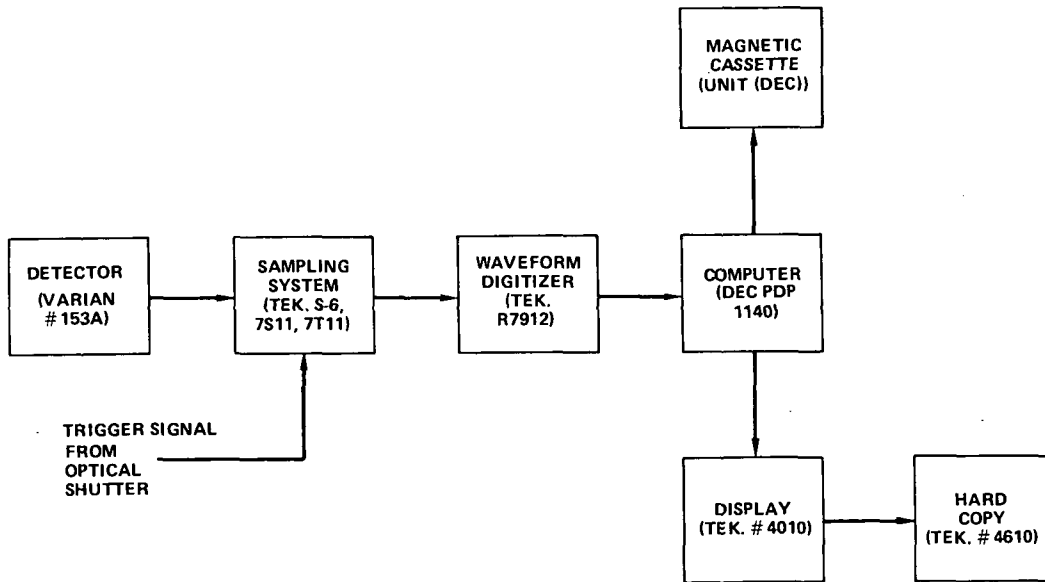


Figure 16. Detection and data processing.

The detector output signal, along with a synchronized trigger signal from the transmitter shutter, was sent to a Tektronix sampling system. The sampled analog waveforms developed at this point were digitized by a Tektronix R7912 and stored in the computer. The R7912 supplied waveforms to the computer at a rate of about 10 per second. Typically, for a given set of test parameters, 200 waveforms were input to the computer; they were averaged by the computer; and the resultant waveform was delivered to the three outputs (that is, magnetic tape, cathode ray tube display, and hard copy). Following the data taking, the averaged waveforms were recalled from the cassettes and analyzed in terms of pulse shape characteristics and, in those cases where both the Geos and reference arrays were illuminated, interpulse spacing.

Pulse Spreading

The physical mechanism that is responsible for pulse spreading is shown schematically in figure 17. When a single laser pulse is incident on the satellite, each cube corner reflects a signal independently of all other cube corners. Therefore, the return signal is a train of pulses; the temporal spacing between pulses is determined directly by the geometry of the array and the amplitudes are determined by the effective aperture of the individual reflectors (since cube corners operating off-normal have less effective area than those at normal incidence). Disregarding waveform variations due to coherency effects,* the photodetector output signal can be considered as the convolution of its impulse response (line c, figure 17) with the return pulse train (line b);† this output signal is clearly much wider than that which would be obtained from either a single cube corner, or a flat array of the cube corners aligned normal to the incident beam.

Average return waveforms from a typical data run for the Geos-3 array at incidence angles from 0 degrees to 65 degrees are shown in figure 18 a through i, with the system response given by j. Pulse broadening in excess of that shown in j must be attributed to the satellite array since all other elements of the measurement are the same in each case. It is important to note that essentially all the return signal from the satellite was detected in this case since the receiver field of view was about 10^4 radians. Table 5 lists the rise time (10 percent to 90 percent), the fall time (90 percent to 10 percent), and pulse width, (FWHM‡) for both the satellite and reference arrays.

Making the usual linear systems assumption that measured rise and fall times are the root of the sum of the squares of the individual contributors in the system, the rise and fall times contributed just by the satellite array have been calculated and are listed in table 6.

These data can be used for calculations of receiver pulse characteristics for transmitter pulses of arbitrary rise and fall time.

*The relative phase angles associated with the optical fields of adjacent pulses are typically on the order of 10^5 radians. Since it is not practical to obtain the phase angle between the individual reflectors with precision of an optical wavelength, the pulses in the return signal must be considered to be randomly phased. At those points in time where two or more pulses overlap (for example, pulses 6 and 7 on figure 17), the resultant amplitude depends on the relative phase difference. Since this quantity is probabilistic, the pulse shape becomes random. The average pulse shape, however, is the same as would be obtained by incoherent addition of signal energy. The experimental results reported in this document are based on average waveforms, and therefore cannot be used to infer the pulse-to-pulse waveform variations resulting from coherent effects. Such data have been obtained by P.O. Minott using digital computer models of the system, and are available on request.

†In a rigorous sense, that is true only for the case of very high optical signal-to-noise ratios (SNR). At low signal levels, the randomness induced by poissonian photoemission causes another degree of randomization of the output waveform. The data reported here result from averaged waveforms built up using large numbers of optical pulses (typical 10^4). This averaging is equivalent to operating at very high SNR.

‡FWHM = Full width at half maximum.

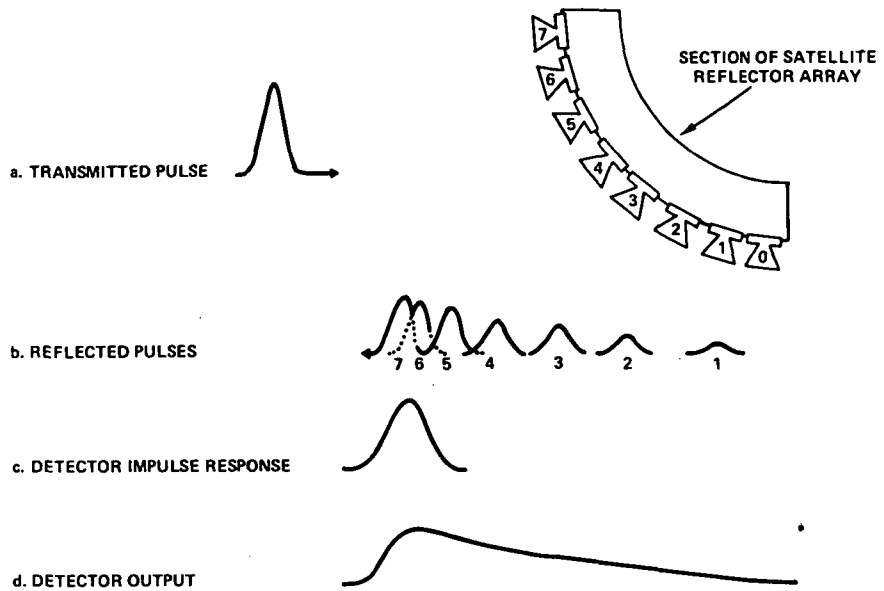


Figure 17. Array-induced pulse spreading.

Table 5
Measured Geos-3 Pulse Characteristics

Satellite Array Orientation degrees	Rise Time (ps)	Fall Time (ps)	Width FWHM (ps)
0	440	480	580
10	430	670	630
20	400	810	720
30	400	930	760
40	410	1020	780
45	410	1020	760
50	390	1030	720
60	420	930	700
65	400	930	660
Reference Array	320	490	380

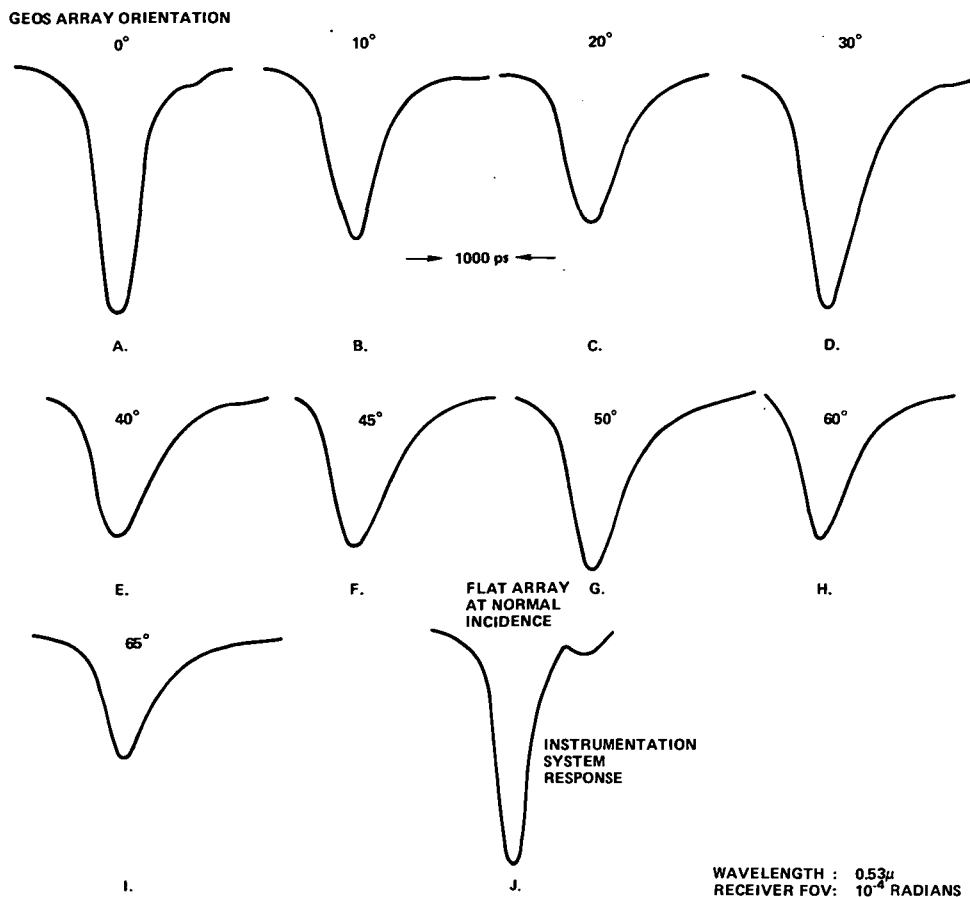


Figure 18. Geos-3 average pulse response.

The discussion of the pulse broadening mechanism presented in connection with figure 17, as well as the test data presented in figure 18 and tables 5 and 6 assumes that the detector receives all the energy reflected from the satellite. In fact, operational tracking systems have aperture sizes of less than 1 m, and the spot size on Earth of the satellite returns is generally a few hundred meters. Therefore, a series of pulse spreading tests were carried out using receiver fields of view as small as possible.*

The location of this quasi-point receiver in the far-field pattern of the return beam is also important since velocity aberration effects cause ground-based receivers to operate 25 to 50 μ r off the axis of the reflected beam pattern. In these tests, the quasi-point receiver was located at four different positions in the far-field pattern in the 25 to 50 μ r annulus, and the results that are presented represent averages for the four positions.

Table 7 lists the pulse width measurements and compares them to the large field-of-view (FOV) results presented earlier. (Results for array orientation of 0 degrees, 10 degrees, and

*The lower limit on receiver field of view being determined by the optical SNR at the input of the photodetector.

Table 6
Array-Induced Pulse Spreading

Satellite Array Orientation degrees	Rise Time (ps)	Fall Time (ps)
0	290	---
10	290	460
20	230	650
30	240	790
40	250	890
45	250	900
50	220	910
60	270	800
65	230	800

65 degrees were not obtained due to insufficient optical SNR.) A reduction in pulse width, amounting to as much as 140 ps, is apparent. Additional analysis indicated that this reduction in pulse width is due to a change in fall time of the received pulse, with the rise time essentially unchanged from the large FOV case.

The mechanism responsible for this change in fall time can be explained by referring to figure 17. For the large FOV case when essentially all the return signal is captured by the photodetector, the relative magnitude of the reflected pulses is shown in line b, and the detector output is shown in line d. In the small FOV case, the detector is receiving signal through a "point" aperture located at a specific position in the far-field pattern of the return signal. This far-field pattern is, in fact, the summation of the far-field patterns from the individual cube corners, each cube corner acting as an independent radiator with its own antenna gain. The antenna gain (or equivalently, the beam divergence of the reflected signal) of the individual Geos-3 cube corners depends on two factors: first, the dihedral angle offset intentionally built into the reflectors to accommodate the velocity aberration; and second, the usual laws of diffraction theory. At the appropriate points in the far field (that is, 25 to 50 μ r off-axis), the antenna gain of a Geos-3 cube corner decreases as the angle of arrival of the incident signal increases; this decrease is due primarily to diffraction. In effect then, the antenna gain associated with the signal leaving reflector #1 (figure 17) is significantly less than that associated with reflector #7. Therefore, a representation of the received pulse train as seen by a "point" detector in the far field would differ from that of line b in that

Table 7
Pulse Spreading for Point Receiver

Satellite Array Orientation	Pulse Width (FWHM, ps) Large FOV	Pulse Width (FWHM, ps) Small FOV
0°	580	---
10°	630	---
20°	720	580
30°	760	660
40°	780	640
50°	720	660
60°	700	700
65°	660	---

the trailing pulses (1, 2,) would be deemphasized with respect to the leading pulses. This, of course, is responsible for the reduction in fall time noted in the experiment measurements.

Range Correction for Center of Mass Tracking

The ranging measurements obtained by ground-based laser systems while tracking in-orbit satellites are, in fact, distance measurements between a well-defined point in the ground station optical system and a rather vaguely defined point near the surface of the satellite reflector array. In order to make full use of the precision available in such data, it is generally desirable to relate the range measurement to the center of mass of the satellite, since it is this point whose motion can be calculated through knowledge of the Earth's geopotential field.* Figure 19 shows that the range correction for a gravity gradient stabilized satellite (for example, Geos-3) is generally a function of the orientation of the vehicle with respect to the incident beam (γ); for the gravity gradient stabilized case γ can be calculated from knowledge of the ground station pointing angle θ and orbital altitude h . Therefore, the prelaunch measurement requirement reduces to evaluating the range correction as a function of γ , the angle of incidence. The technique used to evaluate the range correction is shown in figure 20. A flat reference array is mounted a known distance (R_2) in front of the satellite array, and therefore each incident pulse results in a pair of reflected pulses. By measuring the temporal spacing (ΔT) between the two reflected pulses, and knowing the location of the Geos array with respect to the satellite CG(R_1), the range correction can be evaluated

*Or, inversely, the Earth's gravity field can be calculated from the corrected range measurements.

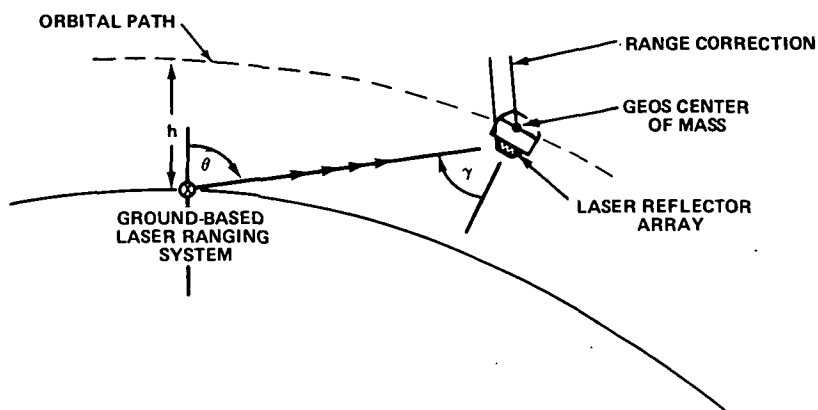


Figure 19. Concept of range correction for center of mass tracking.

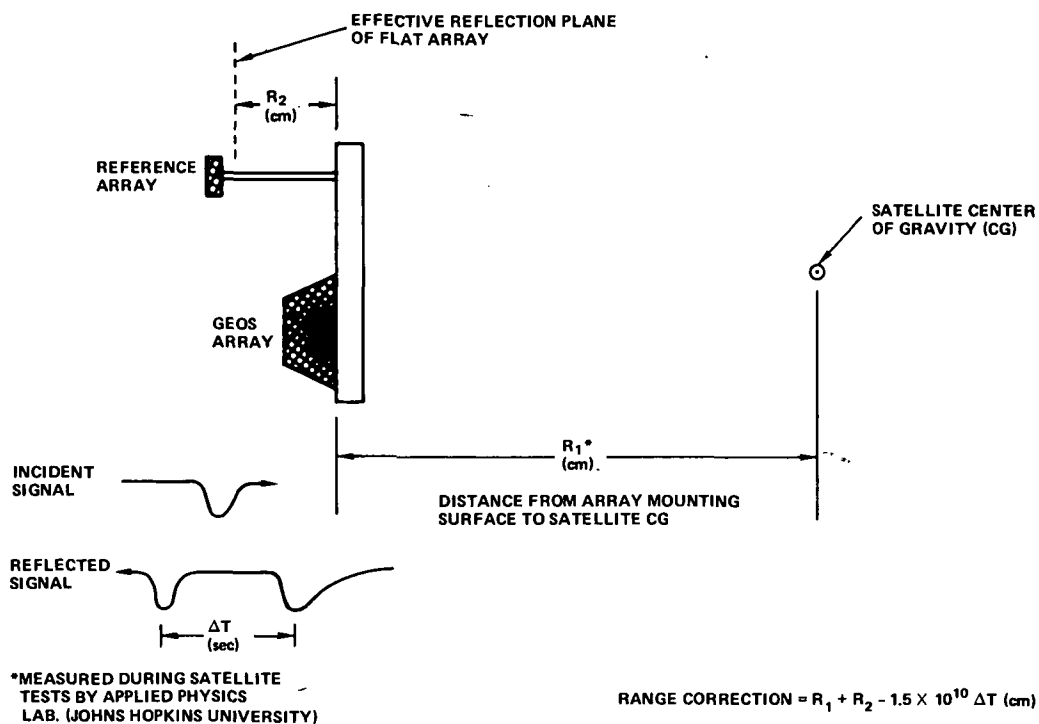


Figure 20. Measurement technique for range correction.

as shown in the figure. Data were taken for angles of incidence (γ) from 0 to 65 degrees; however, in each case, the reference array was maintained normal to the incident signal so that its effective reflection plane was precisely defined. The results are summarized in table 8.

The second column lists the experimental values with the negative sign implying that the effective reflection plane of the array is in front of the satellite center of gravity (CG). A

Table 8
Range Corrections for Geos-3

Incidence Angle (degrees)	Experimental* $\lambda = .53 \mu\text{m}$	Range Correction - Meters* "Retro" Program $\lambda = .6943 \mu\text{m}$	algorithm**
0	-1.316	-1.3050	-1.304
10	-1.355	-1.3960	-1.350
20	-1.367	-1.3770	-1.379
30	-1.356	-1.3653	-1.366
40	-1.291	-1.3167	-1.314
45	-1.273	-1.2769	-1.272
50	-1.221	-1.2236	-1.219
60	-1.084	-1.0833	-1.085

*Centroid detection was used in the experimental measurements and the RETRO program calculations.

**Range correction = $[1.411 - 0.36 (\gamma/\gamma+3)] \cos (\gamma - 22.473)$ meters.

digital computer model of the array was also constructed and evaluated using the RETRO program recently developed by Minott at GSFC. These results are listed in the third column and are clearly in excellent agreement with the measurements. An algorithm that fits the results with about 1-cm accuracy is also shown in the table; this may be useful in computerized reduction of tracking data. Both the experimental and analytical results listed here apply to the 0.53- μm wavelength. However, operation at other wavelengths (such as 0.69 μm) is not expected to change the results by more than a few millimeters.

It should also be noted that the experimental results were obtained with the large field-of-view (FOV) receiver system (so as to enhance the SNR). Operation with a point receiver would change the received pulse shape slightly by reducing the fall time (as discussed in the section, "Pulse Spreading"). The net effect of this would be to move the centroid of the pulse forward a few millimeters; incorporation of this effect into the measurements would decrease the small difference between the measured and analytical results even further. Figure 21 plots the range correction as a function of incidence angle γ and the ground station zenith pointing angle θ .

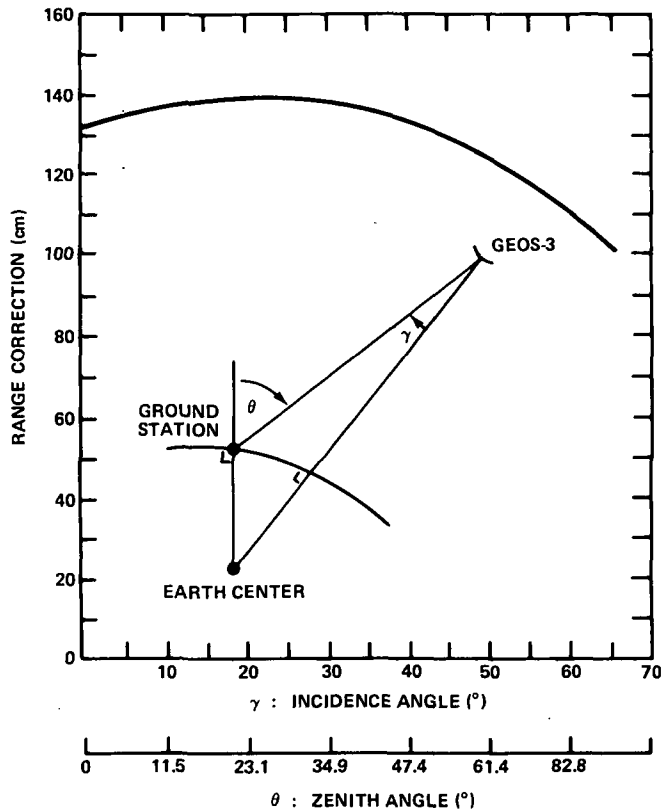


Figure 21. Geos-3 laser range correction.

If the satellite maintained a perfect local vertical orientation throughout its orbit (by use of the gravity gradient stabilization system), then the incident angle γ could be calculated precisely from knowledge of the ground station "look" angle θ , and each range measurement could be "corrected" using the data of figure 21. However, there is a potentially significant amount of error in attitude stabilization systems that causes the instantaneous attitude to jitter about the nominal (that is, desired) value. Since the instantaneous attitude generally is not known, this mechanism represents a residual error source. The magnitude of this error source is shown in figure 22, which is a numerical differentiation of figure 21. The Geos-3 attitude stabilization system is expected to achieve local vertical orientation to much better than a degree, so this particular error source should be maintained at less than 1 cm throughout the orbit.

Summary/Target Signature Tests

In summary form, the results of the Geos-3 target signature tests are as follows:

- (1) The laser reflector array spreads incident pulses by increasing the rise time by about 250 ps and the fall time by about 800 ps (see table 6).

- (2) The range correction has been evaluated experimentally and was found to agree with computer models to within about 1 cm.
- (3) Error introduced into the range correction by spacecraft attitude instabilities can be kept below 1 cm assuming a spacecraft stability slightly better than ± 1 degree.

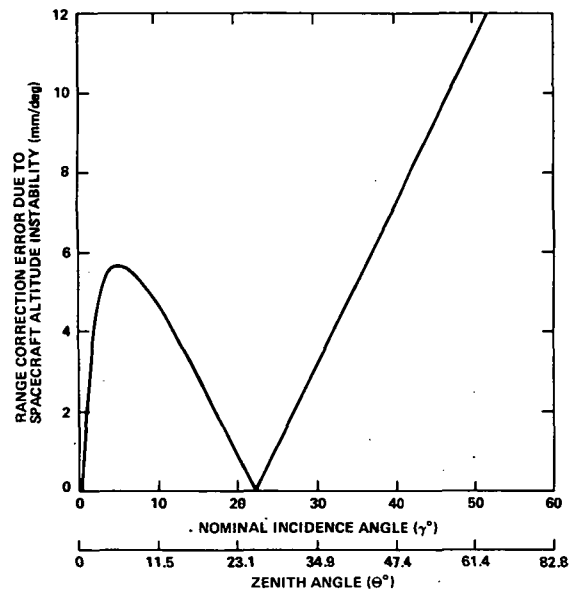


Figure 22. Range correction error due to spacecraft attitude instability.

ACKNOWLEDGMENTS

The authors wish to acknowledge and thank their coworkers at the Goddard Space Flight Center who participated so enthusiastically in the planning and implementation of this program. Special recognition is due the members of the Test Team, including Thomas Depuy, Don Premo, and Mona Tycz of GSFC and David Grolemond of RCA. Funding resources to carry out this work were supplied by Chris Stephanides of GSFC, whose early recognition of the importance of these tests was instrumental to their genesis.

Goddard Space Flight Center
 National Aeronautics and Space Administration
 Greenbelt, Maryland December 1977

SOURCES

- Minott, P. O., "Analysis of Requirements for Geos-C Laser Cube Corner Reflector Panels," TM X65862, January 1972.
- Minott, P. O., "Design of Retrodirector Arrays for Laser Ranging of Satellites," TM X70657, March 1974.
- Minott, P. O., "Measurement of the LIDAR Cross Section of Cube Corner Arrays for Laser Ranging of Satellites," TM X70863, September 1974.

APPENDIX A

CUBE CORNER AND ARRAY SPECIFICATIONS

APPENDIX A CUBE CORNER AND ARRAY SPECIFICATIONS

1.0 SCOPE

This specification establishes the requirements for cube corner reflectors (prisms) which will constitute the optical portion of laser retroreflector panels that will be installed on the Geos-3 spacecraft. Their specific function will be to reflect laser pulses originating on the Earth back to an Earth stationed receiving telescope. The cube corners will be attached in some manner to a fiberglass-nylon phenolic honeycomb substrate, which in turn will be mounted to the Earth-facing side of the spacecraft.

2.0 APPLICABLE DOCUMENT

2.1 APL Drawing No. C-7234-1076, Cube Corner Geos-3 Spacecraft.

3.0 REQUIREMENTS

3.1 General

These cube corners will be used in a space application and therefore will be subjected to vibration and loading conditions peculiar to a launch environment, significant temperature extremes, and the vacuum associated with a near Earth orbit. The cube corners, although exposed to direct Sunlight at times, for the most part, will be looking at the Earth once the spacecraft becomes operational.

3.2 Physical Properties

3.2.1 *Dimensions:* Each cube corner will be manufactured in accordance with the provisions stipulated in section 2.1 control drawing.

3.2.2 *Material:* Prisms shall be made of homogeneous, radiation resistant fused silica free of strains or striations. The grade shall be equivalent to or better than Amersil Special or Supercil I.

3.2.3 *Coatings:* Reflecting faces shall be coated with silver with a protective overcoat. Reflectivity per reflection internal to the prism shall be 94% or better at 6943 Å. The refractive surface of the prism shall be coated with a hard anti-reflection coating peaked for optimum efficiency at 6943 Å. Net optical efficiency of the prism shall be greater than 75%.

3.2.4 Surface Finish: Each surface shall have a specular finish with a flatness tolerance of 1/10 wavelength for the rms deviations of the surface from a true plane.

3.2.5 Dihedral Angles: All the dihedral angles shall be $90^{\circ} 0' 2'' \pm 0.50''$.

3.3 Workmanship

Each cube corner shall be manufactured, processed, and handled in accordance with currently accepted practices for high quality aerospace components.

4.0 QUALITY ASSURANCE

4.1 Critique of Bulk Material

APL and NASA representatives, in conjunction with the contractor, will critique the bulk material which will be designated for purchase by the contractor from his supplier prior to the purchase.

4.2 Government Source Inspection

The Government reserves the right to perform source inspection at the manufacturer's facility at any point during the fabrication and testing of the cube corners.

4.3 Acceptance Testing

A. Test Procedure

The Contractor shall prepare and submit to APL for approval, an Acceptance Test Procedure. The Procedure shall be sufficiently detailed to demonstrate the contractor's ability to ensure compliance with all requirements of this specification. Suggested methods include the use of a Twyman Green interfereogram or a far field pattern produced by an autocollimator.

B. Acceptance Tests

Acceptance tests shall be conducted on each cube corner, in accordance with the Acceptance Test Procedure. Testing shall not be started until APL written approval of the Procedure has been obtained.

4.4 Data Requirements

The following data shall be supplied with each lot of cube corners shipped:

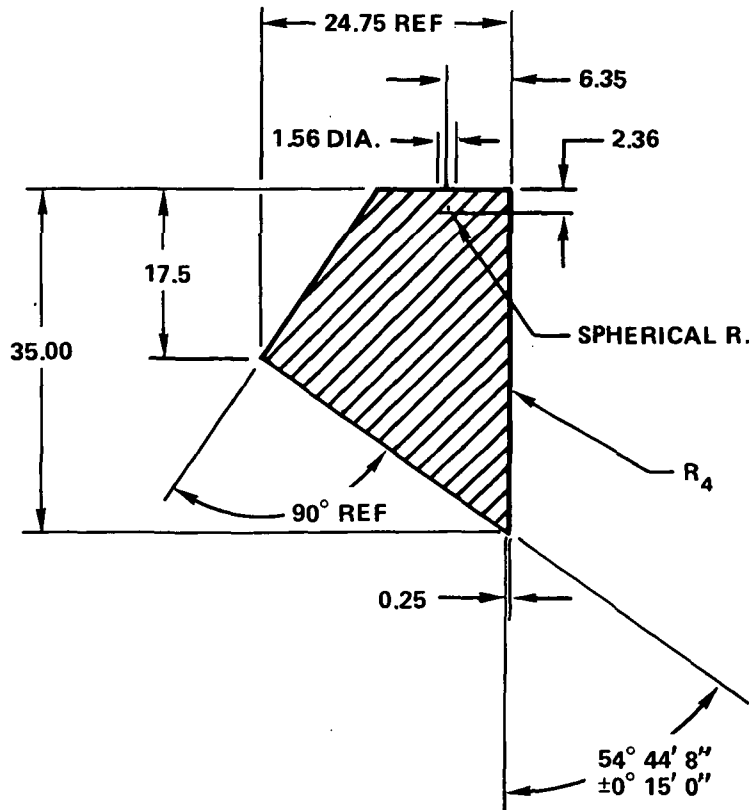
A. Acceptance test data for each cube corner, as required by the approved Acceptance Test Procedure.

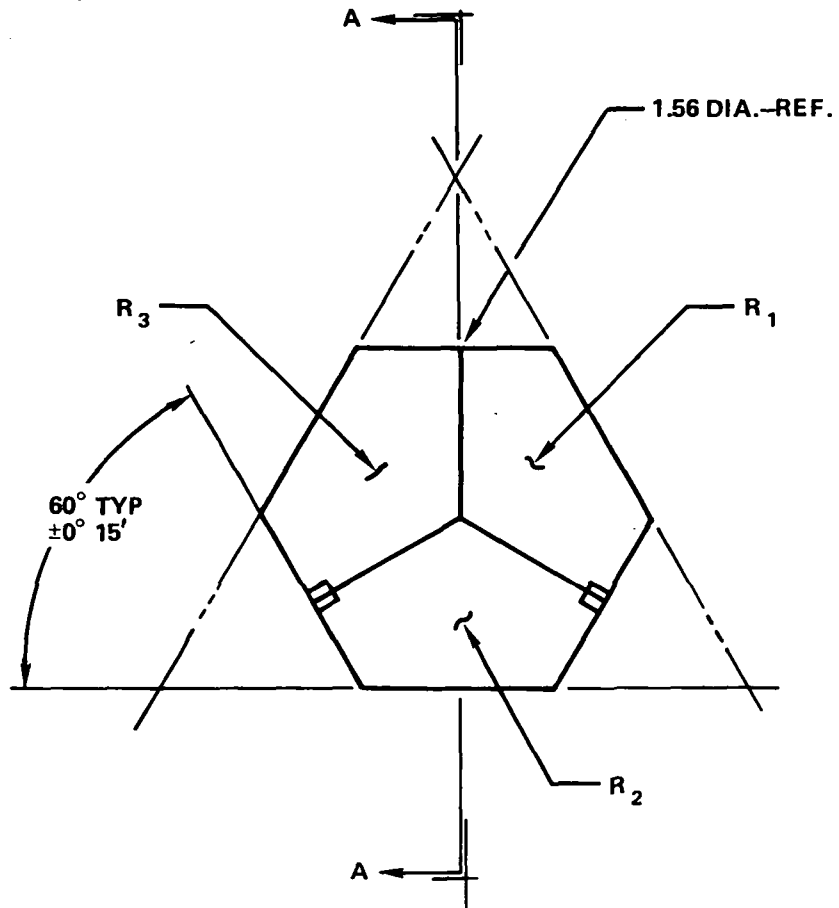
B. Certificates of Compliance for the lot, as follows:

- 1) Certificate, signed by a responsible representative of the contractor, indicating compliance of the delivered cube corners, with all of the requirements of this specification.
- 2) Certificate attesting to the optical quality of the fused silica from which the lot of cube corners has been fabricated.

5.0 DELIVERY

The vendor shall take the necessary precautions to ship the finished cube corners in an acceptable container lined with some type of shock absorbing cushion material.





NOTED:

1. Angles between faces to be $90^{\circ} 0' 2'' \pm 0.50''$.
2. Tolerance on linear dimensions ± 0.25 mm.
3. Minimum protective bevel on all corners and edges.
4. Hard antireflection coating.
5. Material: fused silica, equivalent in optical probe to Amersil special or Suprasil I.

APPENDIX B
THE RADAR RANGE EQUATION

**APPENDIX B
THE RADAR RANGE EQUATION**

The classical radar range equation is as follows:

$$S = \frac{E_T G_T G_R \lambda^2 \sigma}{(4\pi)^3 R^4} \quad (\text{B-1})$$

where

- S = received signal energy
- E_T = energy transmitted by the laser
- G_T = antenna gain of transmitter
- G_R = antenna gain of receiver
- σ = radar (Lidar) cross section of target
- R = slant range of target

However, for a transmitted beam with a Gaussian profile it can be shown that

$$G_T = 32/\theta_T^2 \quad (\text{B-2})$$

where θ_T is the angular divergence of the beam to the $1/e^2$ intensity points. Also, the gain of the receiver is

$$G_R = \frac{4\pi A_R}{\lambda^2} = \left(\frac{\pi D_R}{\lambda} \right)^2 \quad (\text{B-3})$$

where A_R is the area of the receiver and D_R is the diameter of the receiver, which is assumed to have a circular aperture with no obscuration. Obscuration and optical losses will be taken care of by a system optical efficiency. Therefore equation (B-1), after substitution of equations (B-2) and (B-3), becomes the following:

$$S = \frac{1}{2\pi} \cdot \frac{E_T D_R^2 \sigma}{\theta_T^2 R^4} \quad (\text{B-4})$$

But the received signal is usually wanted in photoelectrons, while the transmitted energy is usually in joules. Therefore, a conversion must be made by the following relationship:

$$N = \frac{\eta S}{h\nu} \quad (\text{B-5})$$

where η is the photomultiplier quantum efficiency and $h\nu$ is the energy of a photon. But the energy of a photon is

$$h\nu = \frac{Q}{\lambda} \quad (\text{B-6})$$

where Q is 1.987×10^{-25} joule meters. Therefore,

$$N = \frac{\eta\lambda S}{Q} \quad (\text{B-7})$$

Substituting into equation (B-4) yields

$$N = \frac{1}{2\pi Q} \cdot \frac{\eta\lambda E_T D_R^2 \sigma}{\theta_T^2 R^4} \quad (\text{B-8})$$

However, as yet losses have not been taken into account. To do this, two terms are added: (1) τ_A^2 , to account for the two-way atmospheric absorption, and (2) ρ_0 , to account for all losses in the transmitter/receiver system. Losses in the retroreflector are taken into account in the calculation of σ . Therefore, the final equation becomes

$$N = \frac{1}{2\pi Q} \cdot \frac{\eta\lambda E_T D_R^2 \tau_A^2 \rho_0 \sigma}{\theta_T^2 R^4} \quad (\text{B-9a})$$

A variation that may be used if equation (B-5) rather than equation (B-7) is substituted into equation (B-4) is

$$N = \frac{1}{2\pi} \cdot \frac{\eta E_T D_R^2 \tau_A^2 \rho_0 \sigma}{(h\nu) \theta_T^2 R^4} \quad (\text{B-9b})$$

Atmospheric absorption is usually accounted for with the following equation:

$$\tau_A = \tau_0^{\sec \theta} \quad (\text{B-10})$$

where θ is the zenith angle and τ_A is the zenith atmospheric transmission. The quantity τ_0 is usually taken to be 0.70 at visible wavelengths, but can vary by a large amount due to weather conditions.

The ρ term takes all optical efficiencies of the transmitter and receiver into account and includes a central obscuration factor if the receiver telescope is cassegrainian.

APPENDIX C

GEOS-3 FAR-FIELD DIFFRACTION PATTERNS

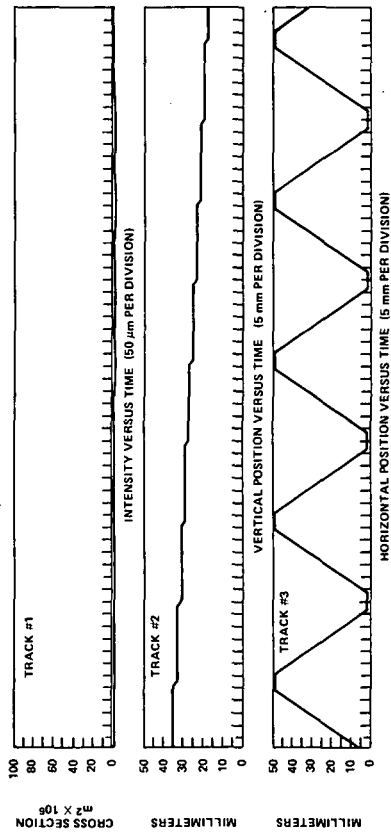


Figure C-1. Geos-3 far-field diffraction pattern for 0° incidence angle.

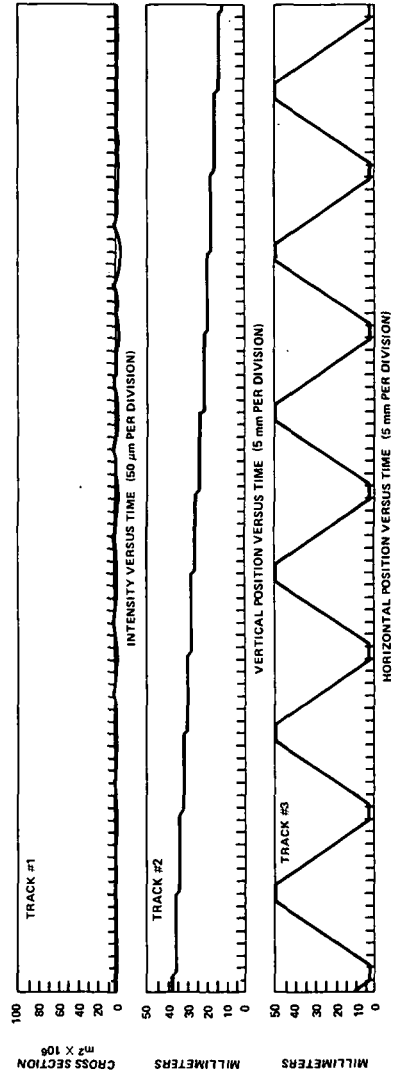


Figure C-2. Geos-3 far-field diffraction pattern for 5° incidence angle.

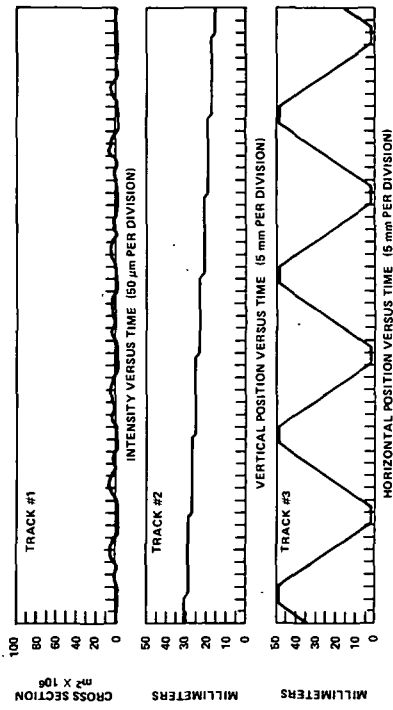


Figure C-3. Geos-3 far-field diffraction pattern for 10° incidence angle.

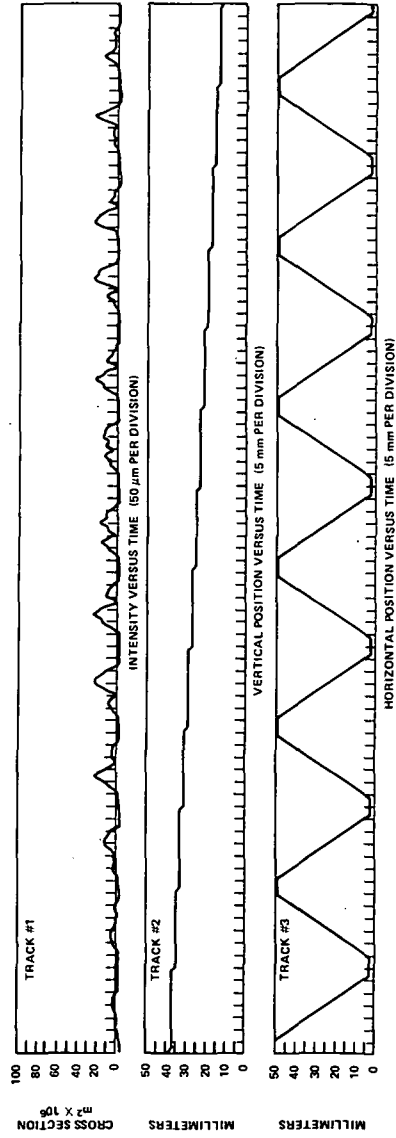


Figure C-4. Geos-3 far-field diffraction pattern for 20° incidence angle.

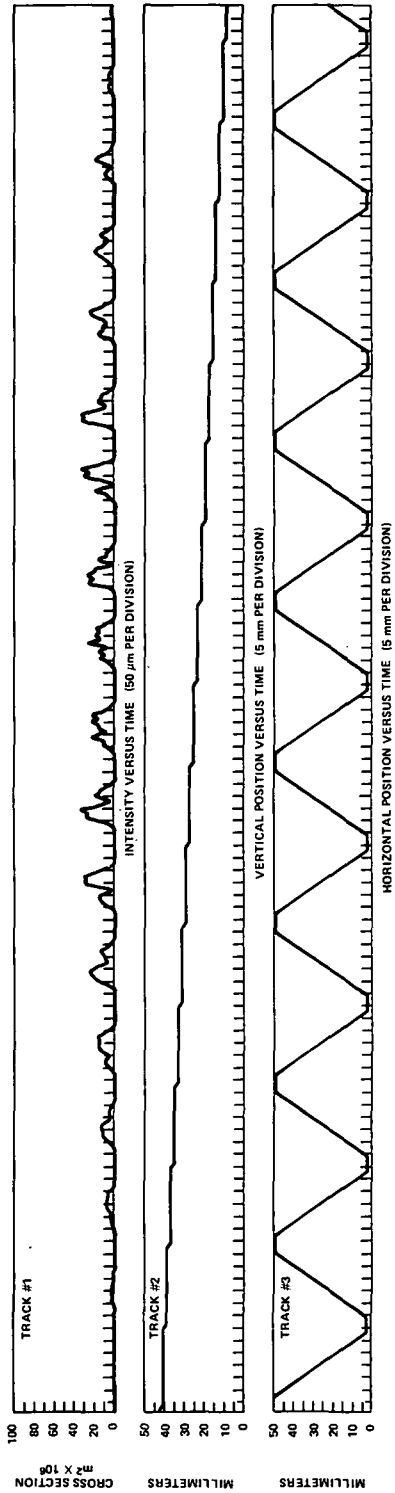


Figure C-5. Geos-3 far-field diffraction pattern for 30° incidence angle.

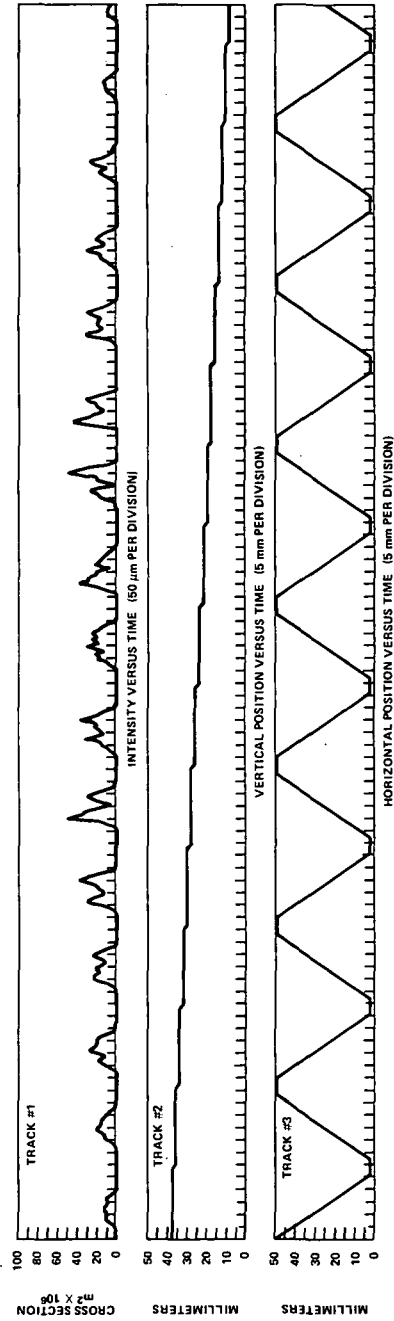


Figure C-6. Geos-3 far-field diffraction pattern for 40° incidence angle.

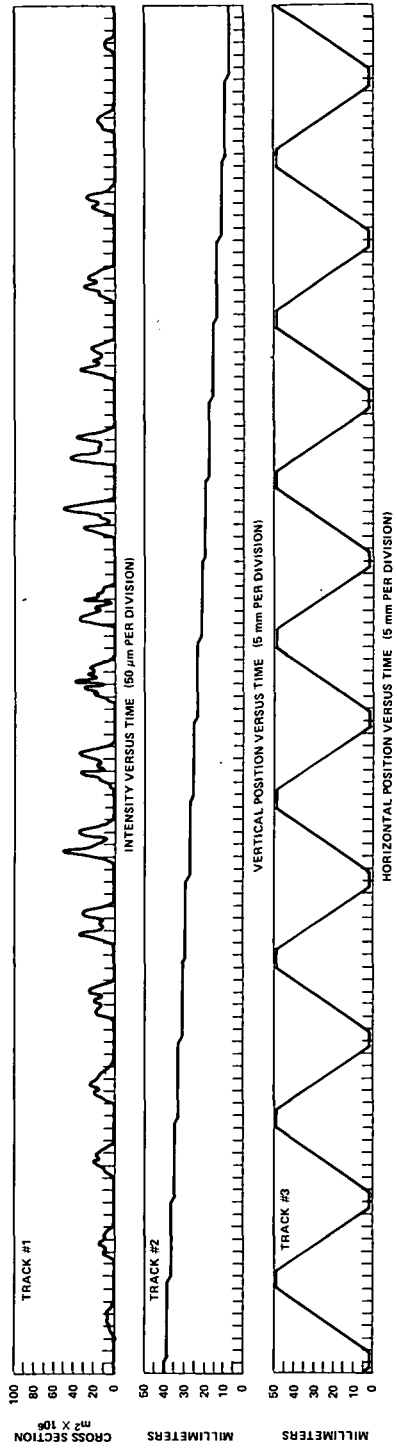


Figure C-7. Geos-3 far-field diffraction pattern for 45° incidence angle.

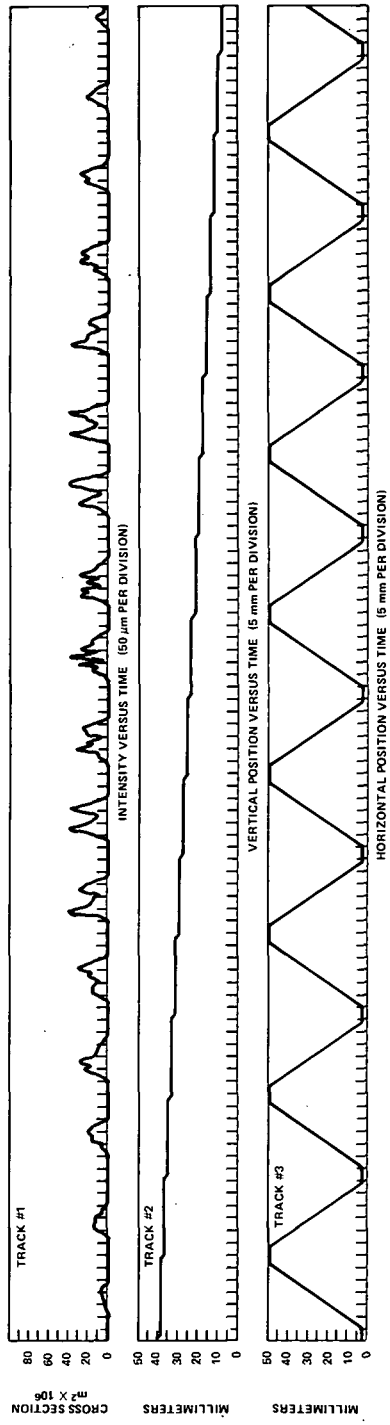


Figure C-8. Geos-3 far-field diffraction pattern for 50° incidence angle.

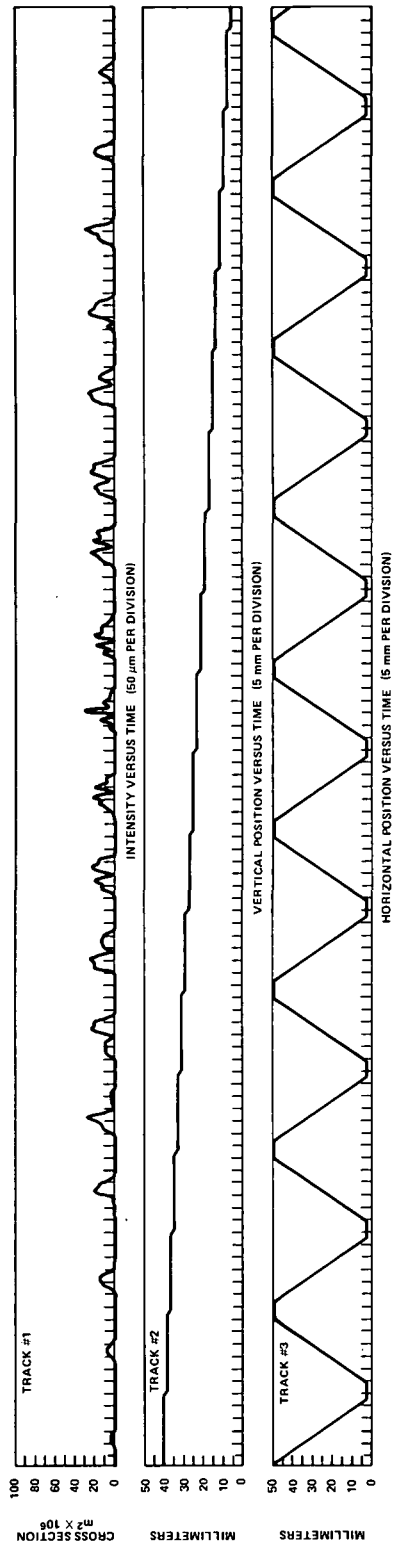


Figure C-9. Geos-3 far-field diffraction pattern for 60° incidence angle.

1. Report No. TP-1138	2. Government Accession No.	3. Recipient's Catalog No.	
4. Title and Subtitle Prelaunch Testing of the Geos-3 Laser Reflector Array		5. Report Date January 1978	
		6. Performing Organization Code 723	
7. Author(s) P. O. Minott, M. W. Fitzmaurice, J. B. Abshire, and H. E. Rowe		8. Performing Organization Report No. G7702-F19	
9. Performing Organization Name and Address Goddard Space Flight Center Greenbelt, Maryland 20771		10. Work Unit No. 506-20-33	
		11. Contract or Grant No.	
12. Sponsoring Agency Name and Address National Aeronautics and Space Administration Washington, D.C. 20546		13. Type of Report and Period Covered Technical Paper	
		14. Sponsoring Agency Code	
15. Supplementary Notes			
16. Abstract This paper describes the prelaunch testing performed on the Geos-3 Laser Reflector Array before launch to determine the lidar cross section of the array and the distance of the center of gravity of the satellite from the center of gravity of reflected laser pulses as a function of incidence angle. Experimental data are compared to computed results.			
17. Key Words (Selected by Author(s)) Retroreflectors, Cube corners, Laser Ranging, Laser Reflectors		18. Distribution Statement STAR Category 36 Unclassified—Unlimited	
19. Security Classif. (of this report) Unclassified	20. Security Classif. (of this page) Unclassified	21. No. of Pages 53	22. Price* \$5.25

* For sale by the National Technical Information Service, Springfield, Virginia 22161

National Aeronautics and
Space Administration

THIRD-CLASS BULK RATE

Postage and Fees Paid
National Aeronautics and
Space Administration
NASA-451



Washington, D.C.
20546

Official Business

Penalty for Private Use, \$300

NASA

POSTMASTER: If Undeliverable (Section 158
Postal Manual) Do Not Return
